Probabilistic Seismic Analysis of an LNG Subplant

Oreste S. Bursi[a*], Rocco di Filippo[a], Vincenzo La Salandra[a], Massimiliano Pedot[a], Md S. Reza[b]
[a] Department of Civil, Environmental and Mechanical Engineering, University of Trento
Via Mesiano 77, 38123, Trento, Italy
oreste.bursi@unitn.it, rocco.difilippo@unitn.it, Vincenzo.LaSalandra@unitn.it, m.pedot@studenti.untin.it

[b] Ingenieurgesellschaft Dr.-Ing. Fischbach Mbh
An der Vogelrute 2 - D-50374 Erftstadt- Lechenich, Germany
rs@ig-fischbach.de

ABSTRACT

Refrigerated liquefied gas (RLG) terminals that are part of lifeline facilities must be able to withstand extreme earthquakes. A liquefied natural gas (LNG, ethylene) terminal consists of a series of process facilities connected by pipelines of various sizes. Although tanks, pipes, elbows and bolted flanges have been a major concern in terms of seismic design, generally, they have not been analysed with modern performance-based procedures. In this study, the seismic performance of pipes, elbows and bolted flanges is analysed and seismic fragility functions are presented within the performance-based earthquake engineering framework.

Particular attention was paid to component resistance to leakage and loss of containment even though several different limit states were investigated. The LNG tank, support structures and pipework, including elbows and flanges, were analysed with a detailed 3D finite element model. For this purpose, we developed a mechanical model of bolted flange joints, able to predict the leakage limit state, based on experimental data. A significant effort was also devoted to identification of a leakage limit state for piping elbows, and we found the level of hoop plastic strain to be an indicator. Given the complexity of the FE model of the LNG plant, we selected the Cloud method for probabilistic seismic demand analysis, due to its advantages in terms of consistency in the seismic input and of computational savings. Then, using a series of nonlinear time history analyses, we studied the behaviour of critical components such as elbows and bolted flange joints. In order to develop fragility curves, we selected a set of 36 ground motions from a database of historic earthquake accelerations. The results of seismic analysis show that bolted flange joints remain significantly below their leakage threshold whilst elbows at the top of the LNG tank are likely to show leakage. Moreover, fragility functions were computed, based on a linear regression approach, and we deduce that elbows located on the tank platform are relatively unsafe against earthquakes. Finally, the estimated probability of loss of containment was above the probability associated with ultimate limit states involved in structural Eurocodes.

Keywords: Seismic Risk; LNG Plant; Piping network; Elbow; Vulnerability analysis; Leakage; Plasticity.

List of Abbreviations

BFJ	*Bolted flange joint*	*LOC*	*Loss of containment*
COV	*Coefficient of variation*	*MSA*	*Multi-Stripe analysis*
DM	*Damage measure*	*PBEE*	*Performance-based earthquake engineering*
DoF	*Degree of freedom*	*PGA*	*Peak ground acceleration*
DV	*Decision variables*	*PRA*	*Probabilistic risk assessment*
EDP	*Engineering demand parameter*	*PSDA*	*Probabilistic seismic demand analysis*
FE	*Finite element*	*PSDM*	*Probabilistic seismic demand model*
IDA	*Incremental dynamic analysis*	*RLG*	*Refrigerated liquefied gas*
IM	*Intensity measure*	*TES*	*Twice elastic slope*
LNG	*Liquified natural gas*		

1 Introduction

1.1 Background and Motivation

Refrigerated liquefied gas (RLG) terminals represent strategic infrastructure for energy supplies all over the world. They play an important role in the overall energy cycle, as their main purpose is to store and distribute RLG. For storage and transport by trains, ships and pipelines, natural gas like ethylene is liquefied. This is achieved by compression and cooling to low temperature. For these reasons, liquefied natural gas LNG terminals usually consist of a port and transport infrastructure, with all the systems related to both liquefaction and regasification, as shown in Fig. 1. In this respect, LNG handles 10% of the global energy supply with 28 LNG terminals in Europe (GIE LNG Map, 2015).

Together with a clear strategic importance, LNG plants also carry a significant risk related to possible consequences of incidents caused by natural events. The Na-tech risk is a central aspect in different types of petrochemical plants due to possible damage to other nearby plant and communities, or to those who rely on them for energy or other needs. Moreover, leakage of hazardous or polluting substances can badly affect the local environment. The resulting hazard has been evaluated in different situations by means of case studies (Cozzani et al. 2014, Baesi et al. 2013, and Young et al. 2005). The considerable variability of seismic events and the related domino effects have been partly taken into account in the overall hazard estimation by the application of complex methodologies (Campedel et al., 2008 and Antonioni et. al., 2007). Nevertheless, historic data shows that earthquakes can lead to severe losses due to the failure of different components of industrial plants; in this respect see Lanzano et al., (2015) and Krausmann et. al (2010).

An industrial plant typically has many structural and mechanical components, with different resistance thresholds and different failure behaviours. One of the most dangerous failure effects is loss of containment (LOC) or leakage, which can lead to explosion, fire and environmental damage. An LNG plant includes a number of component types that can experience leakage, under certain conditions of stress and strain caused by a seismic event. Common vulnerable components of LNG pipelines are bolted flange joints (BFJs) and piping bends or elbows. With respect to BFJs, current European regulations, like EN 1591-1,2 (2009), do not have tools to predict leakage. Moreover, studies whether focusing on leak-before-break, i.e. that concentrate on the steady growth of through-cracks in pipes (Xie, 1998) or tracing the plastic behaviour of elbows (Li and Mackenzie, 2006), do not predict leakage thresholds. To fill this gap, a practical predictive model based on EN 1591 (2009) was developed by La Salandra et al. (2016), also using experimental data found by Reza et al. (2014). As far as a probabilistic approach is concerned, the risk estimation of leakage events is usually based on historic evidence found in databases; for a review, see Barros da Cunha (2016).

In order to quantify induced seismic risk in an LNG plant, a seismic Probabilistic Risk Assessment (PRA) approach suggested by IAEA (2009) for nuclear power plants (NPPs) is available. The procedure is as follows: i) Seismic hazard analysis; ii) Fragility analysis; iii) System analysis and consequence evaluation. The outcome of a seismic PRA includes seismic hazard of the site, the structural capacity of structures and equipment, incorporation of uncertainties in seismic hazard, structural fragility and response of components. Hoseyni at al., (2014) applied a variant of this approach to take into account soil-structure interaction effects. However, this approach is not directly applicable to (non-nuclear) LNG plants, because data on aleatory randomness and epistemic uncertainties in the capacity of LNG components is not available.

As a viable alternative, to rationally quantify the seismic performance of civil facilities, the Performance-Based Earthquake Engineering (PBEE) methodology has been proposed (Cornell and Krawinkler, 2000). This probabilistic framework is based on the prediction of structural behaviour under realistic seismic loadings that the structural system is likely to experience in its reference life. It is based on the combination of different quantities, such as seismic hazard, structural response, level of damage, and repair costs after cyclic loading.

Some examples of application of the PBEE approach can be found in civil engineering literature (Yang et al., 2009, Tondini and Stojadinovic, 2012). Along this line, application of the PBEE approach to petrochemical piping systems by means of codes can be found in Bursi et al. (2015a). Moreover, some applications based on the determination of fragility curves are available for piping systems of NPPs (Firoozabad et al., 2015) and boil-off gas compressors at LNG terminals (Park and Lee, 2015). In both cases, limit states related to leakage were not considered or quantified. Conversely, the selection of engineering demand parameters (EDPs) and corresponding damage levels for piping systems and tanks was carried out by Vathi et al. (2015). Nonetheless, a fragility analysis requires also the analysis of the effects of different intensity measures, e.g. peak ground acceleration (PGA), on the dispersion characteristics of a probabilistic seismic demand model. To the authors' knowledge, this analysis has not yet been carried out for LNG plants.

1.2 Scope

On these premises, this paper presents the application of the fully probabilistic PBEE approach to an LNG plant having a piping system coupled to a support structure and a relevant LNG tank. More precisely, we define limit states and engineering demand parameters related to damage of piping components, i.e. BFJs and elbows. Moreover, among different damage levels, we calculate the correlation between the probability of leakage and the IM of the seismic event represented by the PGA and the spectral acceleration (Sa(T)). We represent these by the mean of fragility curves adopting the Cloud Analysis method (Baker, 2015).

For clarity, the paper is organized as follows: Section 2 presents the methodology for the application of the PBEE method. A description of the LNG plant and the main components modelled by means of finite elements (FEs) is contained in Section 3. Section 4 presents a simple component-based mechanical model able to predict leakage of BFJs and a methodology to evaluate seismic performances of piping elbows. Successively, Section 5 presents a 3D non-linear stick model of the LNG terminal, fully developed in the ANSYS environment (ANSYS, 2015). This FE global model allows for evaluation of the seismic response of structural components of the plant by means of a non-linear analysis presented in Section 6. Thus, the demand model of the main components of the piping system is investigated in the spirit of the PBEE method. Finally, Section 7 draws the main conclusions and future perspectives.

Fig. 1. Refrigerated liquefied gas plant overview

2 Performance-based earthquake engineering procedure

The PBEE procedure was mainly developed by the Pacific Earthquake Engineering Research (PEER) Center and estimates the probabilistic future seismic performance of buildings and bridges in terms of system-level decision variables (DVs), i.e., performance measures that are meaningful to the owner, such as repair cost, casualties, and loss of use -dollars, casualties and downtime-. It is based on four quantities:

- Intensity Measure (*IM*), which represents a measure of the ground motion intensity. Several *IM* variables are available, such as PGA, Spectral Acceleration at the fundamental period (Sa(T)), etc.;
- Engineering Demand Parameter (EDP), which describes the structural response in terms of global and local parameters such as deformation, forces, etc;
- Damage Measure (DM), which identifies the most significant structural damage conditions;
- Decision Variable (DV), which transforms the damage conditions into useful quantities for the risk management decision process.

Let's denote $G(x|y)=Pr(x<X|Y=y)$ the complimentary cumulative distribution function of the considered variables and $dG(x|y)$ the derivative of the conditional complementary cumulative distribution function, which is identical to the negative of the conditional probability density function. The evaluation of the mean annual rate λ of *DV* exceeding the threshold *dv* reads,

$$\lambda(dv < DV) = \int_{im} G(dv|im)\,|d\lambda(im)| \tag{1}$$

where the conditional probability $G(dv|im)$ can be obtained by use of total probability (Yang et al., 2009) as follows,

$$G(dv|im) = \int_{dm}\int_{edp} G(dv|im)dG(dm|edp)\,dG(edp|im) \tag{2}$$

Substituting (2) in (1), we obtain the mean annual rate of a decision variable DV exceeding a threshold value *dv,*

$$\lambda(dv < DV) = \int_{im}\int_{dm}\int_{edp} G(dv|im)dG(dm|edp)dG(edp|im)\,|d\lambda(im)| \tag{3}$$

It is evident that Equation (3) encompasses four components of performance assessment. Specifically, the quantification of $\lambda(im)$ requires a site hazard analysis, usually performed by a probabilistic seismic demand analysis (PSDA); $G(edp|im)$ needs a response analysis, usually performed by using numerical techniques, e.g. Cloud analysis, $G(dm|edp)$ requires a damage analysis often based on experiments whilst $G(dv|dm)$ requires cost-effective or loss analysis (Cornell and Krawinkler, 2000). Moreover, the quantification of Equation (3) requires a fully probabilistic approach. Given the scarcity of data, at this stage of the research, only the probability of exceeding of a certain *edp* will be quantified in Section 6. For this purpose, the following relationship is adopted:

$$P(edp) = \int_{im} P(EDP > edp|im)|d\lambda(im)| = \int_{im} P(D > C_{LS}|IM = im)|\lambda(im)dim| \quad (4)$$

where we introduce the structural demand D and C_{LS}, i.e. the capacity of the component/system associated with a prescribed limit state.

3 LNG Plant

3.1 Introduction

The case study investigated in this paper reproduces a realistic RLG plant, depicted in Fig. 1 and 2, i.e. the Case Study #2 analysed in the European research project INDUSE-2-SAFETY (Bursi et al., 2016b). Originally, this plant was designed for low seismic lateral loads; in stark contrast, in order to acquire additional information on the plant performance for extreme lateral loadings, we considered the LNG plant located in a high seismic-prone area of Priolo Gargallo in Sicily, in the south of Italy. The hazard curve for this site is depicted in Fig. 3 and was calculated within the activities of INDUSE-2-SAFETY (Bursi et al., 2015b). The main component of the plant is a 50 000 m^3 ethylene tank that supplies the LNG to the different process areas via a stainless-steel piping system.

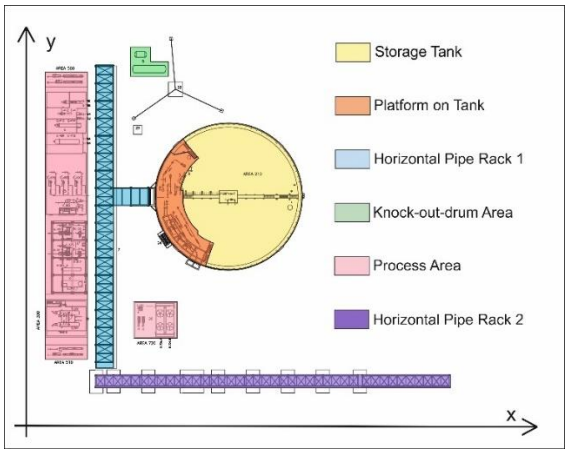

Fig. 2. LNG plant layout

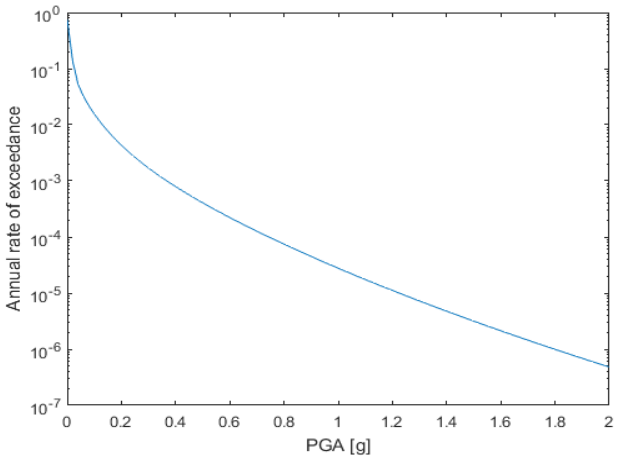

Fig. 3. Hazard Curve of the high-seismic site of Priolo Gargallo (Sicily, Italy).

3.2 LNG Tank

Typically, LNG tanks are used to store LNG at very low temperatures, i.e. -100 °C. A relatively common kind of LNG tank is the full containment tank, where the inner steel tank encloses the LNG and the outer structure is generally thicker and of concrete and includes both an outer steel tank and the insulation material.

The tank of the LNG plant under study, depicted in Fig. 4, has two main different layers: i) the inner one has high resilience steel shells (X8Ni9) of thickness varying from 18 mm for the lower rings to 8 mm for the upper rings and of radius 23 meters; ii) the outer layer is concrete C30/37 with a total thickness of 650 mm. This concrete wall has an inner radius of 24.5 m and a height of 38 m. The roof is a concrete dome, with thickness ranging from 850 to 350 mm, reaching an overall height of 47.4 m.

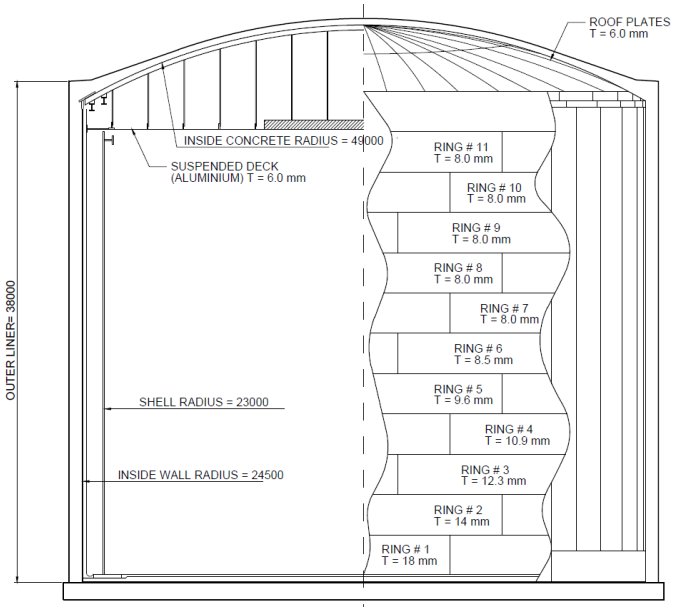

Fig. 4. Main tank layout

3.3 Substructures

Two different structures support the pipework: i) a steel platform located over the dome as shown in Fig. 5, and ii) a concrete structure placed at the base of the tank as in Fig. 6.

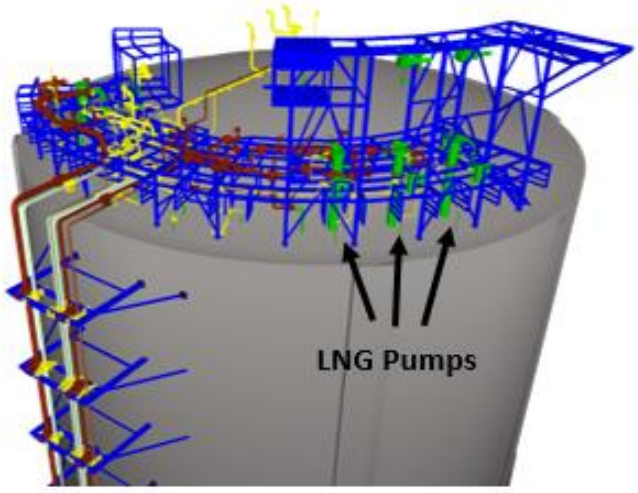

Fig. 5: Steel platform and position of the three pump columns

The platform at the top of the tank is built with 17 different kinds of commercial steel profiles grade S235, arranged on three different levels, located respectively at 41, 45 and 48 m above ground. These steel profiles were selected in the range 100-280 for the HEB profiles and in the range 120-240 for the IPE profiles. Three pumps, located above the dome, transport the ethylene from the tank to the pipework.

At the base of the tank, the piping system distributes ethylene to the different process areas. The pipelines are supported by a concrete structure 102 m long, 6.5 m wide and 7.3 m high with an intermediate level placed 5.3 m above the ground. The span between the columns along the longest dimension is 6 m, whilst the span between the beams along the same direction is 3 m. The concrete compressive strength class is C50/40.

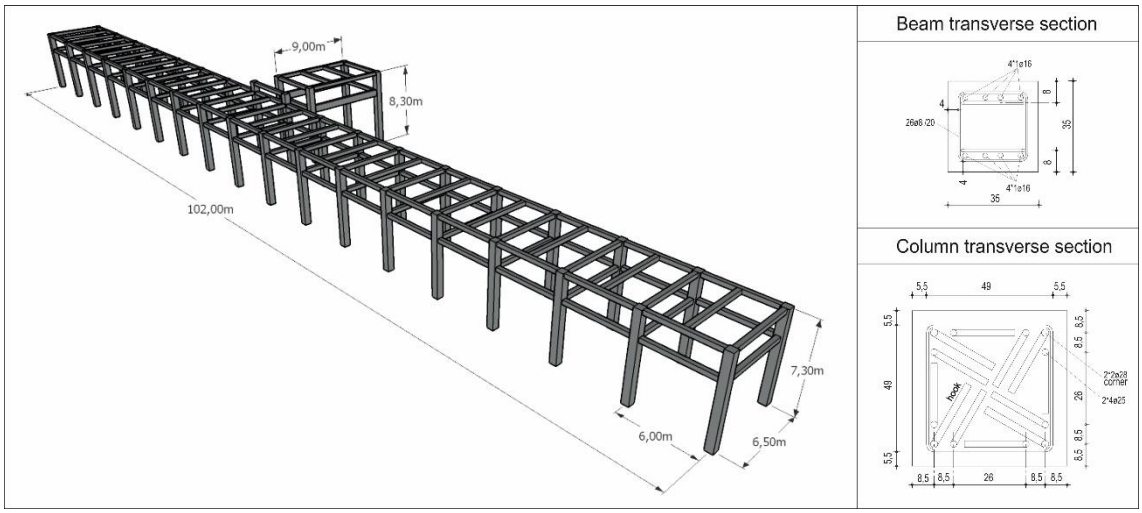

Fig. 6. Concrete support structure

The columns have a 600 mm square section with 8 steel reinforcement bars ϕ25 and 4 steel re-bars ϕ28. The beams are 350 mm square section with 4 steel re-bars ϕ20.

3.4 Knock-Out Drum Area

The knock-out drum process area, the function being to separate liquid from gas in the ethylene mixture, is located at the far end of the concrete support structure as shown in Fig. 2. Separation occurs in two stainless steel tanks,

shown in Fig. 7, connected to the concrete support structure by a piping system for the ethylene supply. The tank considered in the analysis is named C608 and it is highlighted in red in Fig. 7. The vessel dimensions are in Table 1.

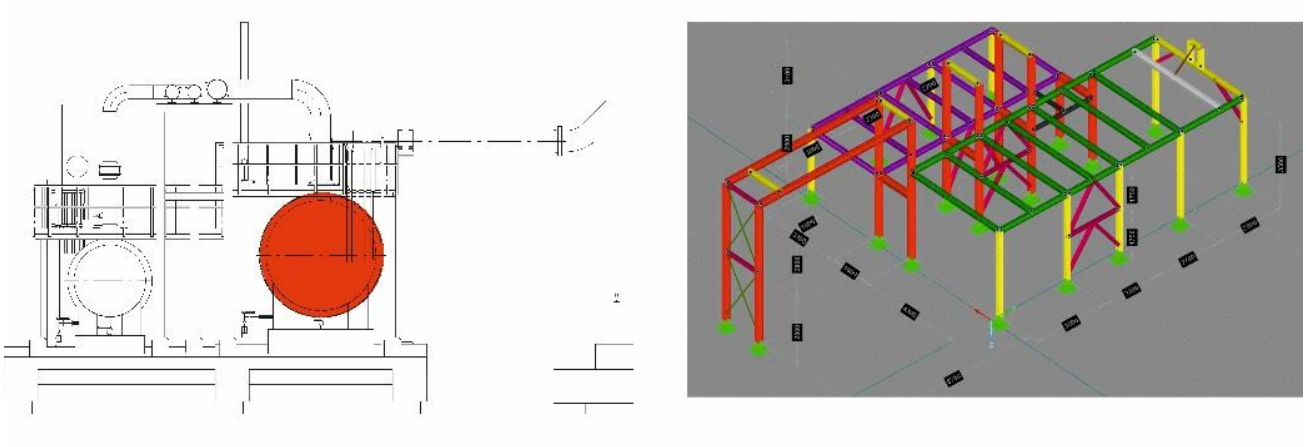

Fig. 7. Knock-out drum process area

Table 1
Properties of Knock-out drum C608 tank

Knock-out drum C608 tank	
Capacity [m^3]	52
Diameter [m]	2.6
Length [m]	10.15
Wall thickness [mm]	8

The two tanks of the knock-out drum area are surrounded by a grade S235 steel support structure that is 17.5 m long, 9.2 m wide and 3.5 m high. The structural steel profiles are in the ranges 120-200 HEB and 160-220 IPE.

3.5 Piping System

The piping system, depicted in Fig. 5 and 8, is arranged into 8 different welded pipelines of stainless steel grade ASTM A312/TP304L.

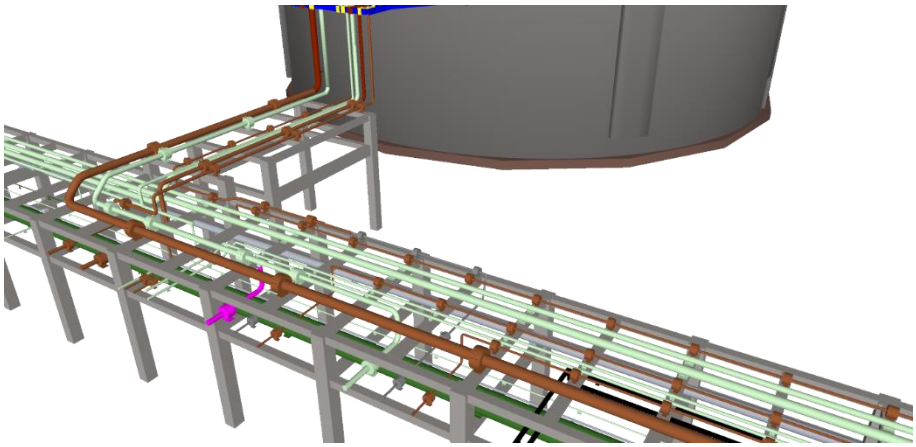

Fig. 8. Pipelines layout on concrete support structure

The cross section properties of each pipeline are summarised in Table 2.

Table 2
Pipeline cross section properties

Cross section properties of the pipelines					
Pipeline number	Pipe specification	External radius [mm]	Wall thickness [mm]	Curvature radius [mm]	Max Operating Pressure [barg]
1	16'' - SCH20	406.4	7.92	610	2.8
2	10'' - SCH10S	273.05	4.19	381	0.2
3	4'' - SCH10S	114.3	3.05	152	0.2
4	6'' - SCH10S	168.28	3.40	229	0
5	12'' - SCH10S	323.85	4.57	457	0.3
6	6'' - SCH10S	168.28	3.40	229	16.3
	8'' - SCH10S	219.08	3.76	305	16.3
7	6'' - SCH10S	168.28	3.40	229	1
8	18'' – SCH10S	457.2	4.78	686	0

The mechanical properties of the pipeline steel were defined during the INDUSE-2-SAFETY project, with experimental tests on metallographic samples of seamless pipes (Bursi et al., 2016a). In order to characterize the steel constitutive law for the operating conditions of the plant, tensile testing was done at room temperature and at -80°C. The relevant results are shown in Fig. 9 and Fig. 10.

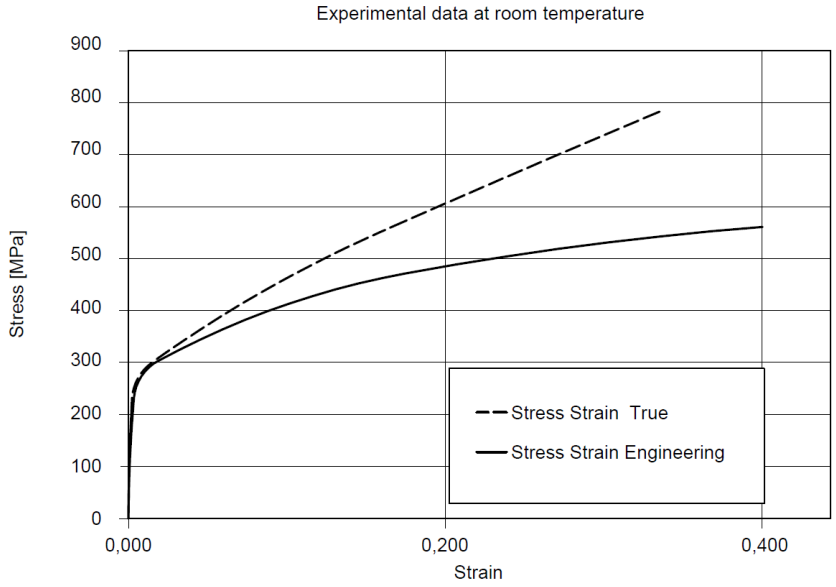

Fig. 9. Stress-strain curve for A312/TP304L at room temperature

Fig. 10. Stress-strain curve for A312/TP304L at -80°C

As expected for steel materials, the A312/TP304L showed a higher elastic modulus and a decrease in ductility at the lower temperature.

The connections between the piping system and other elements such as the pumps over the main tank or the nozzles in the knock-out drum area, are by BFJs. In particular, the connection between pipeline #6 and the three pump columns over the dome of the tank was made with a 6'' SCH10S CL300 welded neck flanges, as shown in Fig. 11. In addition, pipeline #8 and the knock-out drum tank were connected with an 18'' SCH10S CL150 welded neck flange as depicted in Fig. 12.

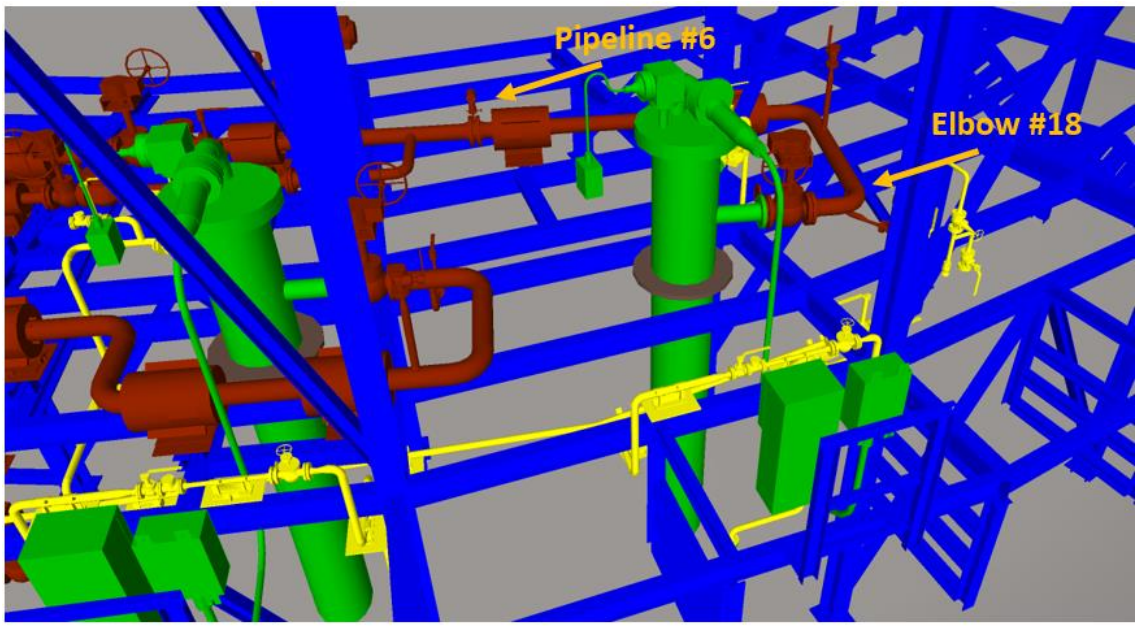

Fig. 11. BFJs connecting the pumps to the piping system

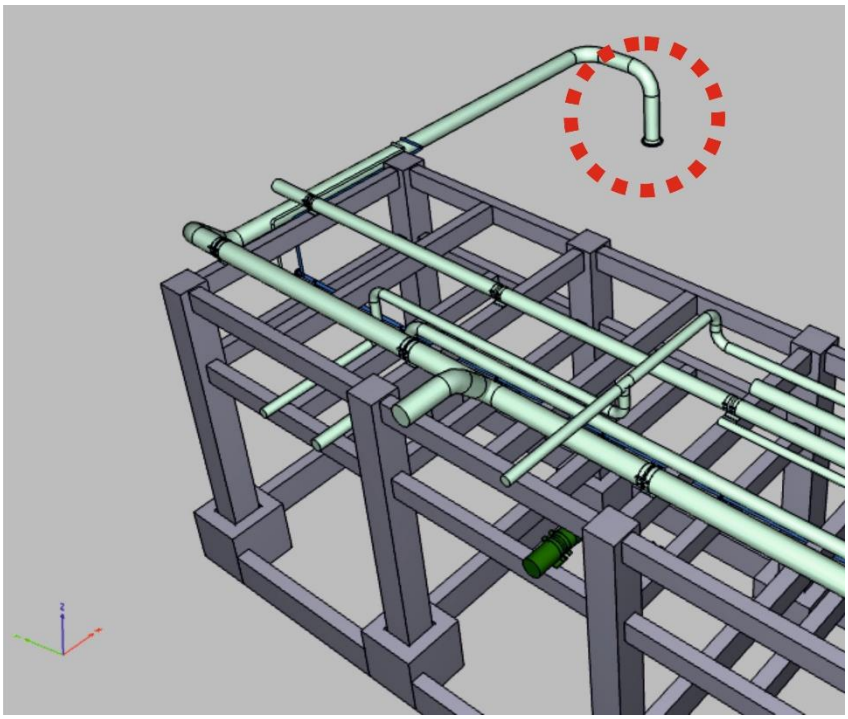

Fig. 12. BFJ between the tank of the knock-out drum and the piping system

4 Critical components for leakage in the LNG plant

Pipelines and their components like BFJs, pipe bends and Tee joints are widely used in LNG plants including the one described in Section 3. With regard to BFJs, these joints are quite complex because they are highly confined statically indeterminate systems and also because they involve a high degree of non-linearity. As a result, it is difficult to correctly estimate their resistance and stiffness, as also the threshold of leakage. They have been investigated in Zerres and Guerot, (2004) and Reza et al., (2014), among others. Here we summarize the research work accomplished by La Salandra et al., (2016), see Subsection 4.1, whose results represent the basis for the mechanical model presented in Subsection 4.2. With reference to pipe bends, they are a vulnerable component of pipelines and we discuss their seismic performance evaluation in Subsection 4.3. Lastly, we do not explicitly mention Tee joints, since only one of them is encompassed into the pipelines. Nonetheless, the experimental campaign carried out allowed for its detailed modelling (Bursi, Reza et al., 2016b). More precisely, the Tee joint did not exhibit a significant stress level being located on the concrete rack, see Fig. 8, at a relatively low height.

4.1 Test campaign and main results

The mechanical model of BFJs was obtained by means of four experimental tests on two different BFJs, both for 8'' pipes, subjected to cyclic and monotonic loading. The two different types of BFJs had flanges of non-standard thickness; in greater detail, thicknesses of 18 and 27 mm (respectively Design 01 and Design 02) were employed, values less than those employed in industry, of the order of 35 mm. Therefore these flanges can be classified as non-standard flanges (Reza et al, 2014). During the test campaign, the BFJs specimens were loaded in the testing equipment depicted in Fig. 13. In greater detail, the joints were located at 45° with respect to the vertical loading axis. The main reason for this choice was the fact that we had no data to predict whether the axial or the shear force would have most influenced the leakage threshold in BFJs. Therefore, we decided to adopt a testing configuration with equal intensity axial and shear forces.

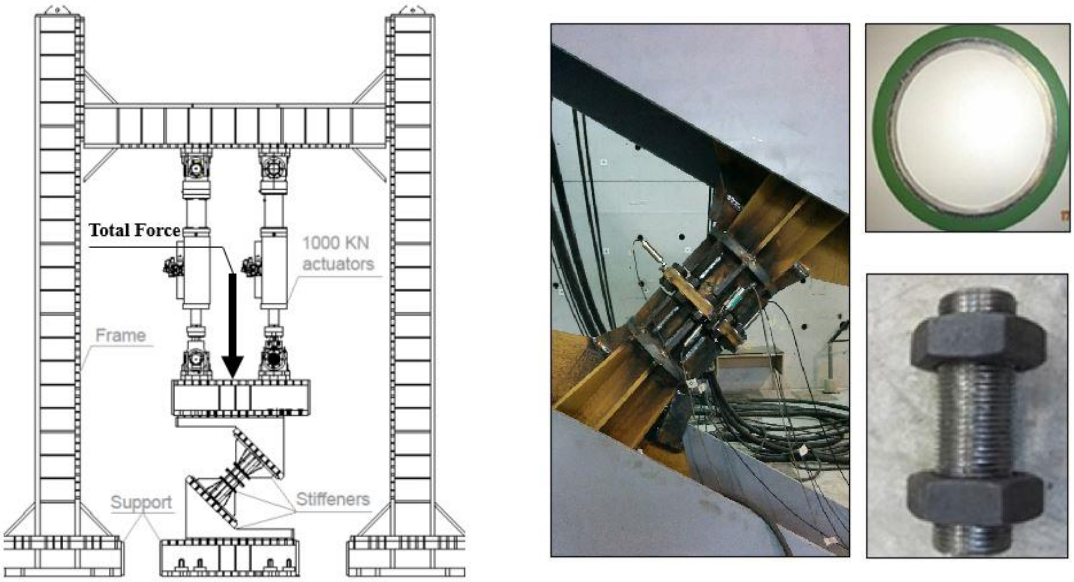

(a) (b)

Fig. 13. (a) BFJ setup. (b) Design 02 specimen, gasket, and a relevant bolt.

Both axial and shear force values corresponding to the onset of leakage are collected in Table 3.

Table 3

Leakage forces for the experimental tests

Specimen Flange Thickness and Loading Type	Leakage Axial Force [kN]	Leakage Shear Force [kN]
18 mm (Design 01) – Monotonic	1175	1175
18 mm (Design 01) – Cyclic	1100	1100
27 mm (Design 02) – Monotonic	1000	1000
27 mm (Design 02) – Cyclic	1470	1470

Although cyclic loading is more severe than monotonic loading for BFJ components, this is not reflected in the leakage forces of Design 02 joints. Moreover, it is worthwhile noting that the onset of leakage corresponds to an inside pressure of 32 bar which is far greater than the internal service pressure in the LNG pipelines, summarized in Table 2.

The corresponding force-displacement relationships are depicted in Figs 14 (a) and 14 (b) for monotonic and cyclic loading, respectively, where the Total Force shown in Fig. 13 (a), is equal to the sum of the forces exerted by the two actuators. These results show that the onset of leakage occurred after first yielding and before plastic collapse.

It is possible to notice that cyclic loading triggered leakage in Design 01 joints, with lower external forces compared to monotonic loading whilst the opposite happened for Design 02. This can be explained considering the differences between the deformation modes of Design 01 and 02. As a matter of fact, Design 01 experiences leakage through the bolts holes with a minimum involvement of flange plates; therefore, the bolts were the components that controlled leakage and similar leakage force levels were exhibited in both monotonic and cyclic loading. Conversely, in Design 02, leakage started from flange plates with a little involvement of bolts. As a result, cyclic loading pre-compressed flange plates increasing their leakage resistance and making the BFJ less vulnerable than that subjected to monotonic loading.

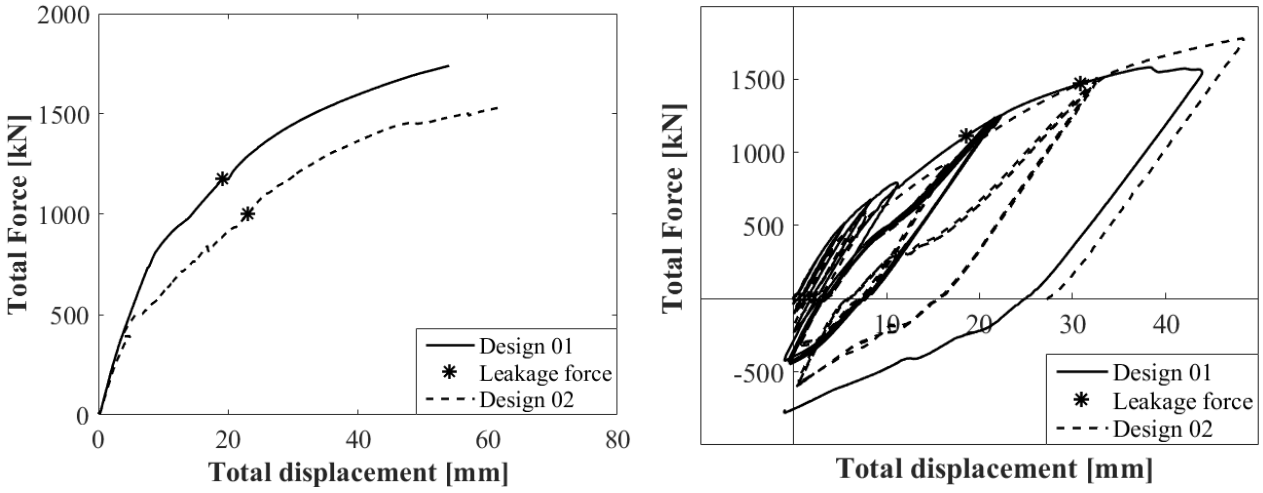

Fig. 14. Load-Displacement diagrams for 18 mm (Design 01) and 27 mm (Design 02) BFJs: (a) Monotonic loading and (b) Cyclic Loading.

4.2 Predictive model for leakage and mechanical model of BFJs

Because pipelines and relevant BFJs of the LNG plant under study are characterized by a variety of diameters, from 4'' to 18'', as listed in Table 2, a mechanical model is needed to predict the onset of leakage for the remaining diameters. To this end, the experimental work of La Salandra et al. (2016) provides the basis for the predictive mechanical model summarized here.

The proposed mechanical model is based on the framework of EN 1591 standard (2009). More precisely, the model considers the BFJ as composed of three main components: bolts, flange and gasket, as reported in Fig. 15, where F_{BI} and F_{GI} define the tensile bolt and the gasket compressive axial forces, respectively; F_{QI} equals the force due to internal pressure whilst F_{RI} represents the resulting external force acting on the joint. Additionally, all these forces are referred to a generic design load condition *I*.

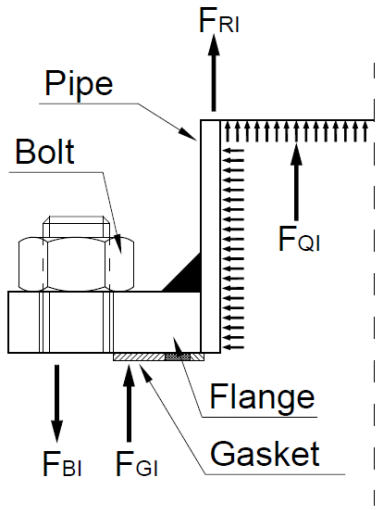

Fig. 15. Bolt, flange and gasket components and force balance in the mechanical model of a BFJ proposed in EN 1591-1 (2009).

This model is based on the assumption that the flange is infinitely stiff in bending, see in this respect Fig. 17, differing from bolts and gasket which can exhibit axial deformation. Moreover, we assume that leakage occurs when the compressive stress on the gasket σ_{GI} is lower than a certain threshold $Q_{s,min,I}^{(L)}$ (EN 1591-1 standard, 2009). Starting

from these hypotheses, the proposed model employs the following equation of the joint compliance at the load condition *I*:

$$F_{GI}Y_{GI} + F_{QI}Y_{QI} + F_{RI}Y_{RI} + \Delta U_I = F_{G0}Y_{G0}P_{QRI} \tag{5}$$

where, F_{G0} defines the gasket compressive force at the initial state *0* - the assembly condition - due to the bolt force tightening, i.e.

$$F_{G0} = \sigma_{G0}A_{Ge} = \sum_{n^\circ\ bolts} F_{tor} = \sum_{n^\circ\ bolts} \frac{M_{torq}}{0.18 * d} \tag{6}$$

After some algebraic manipulations, the pressure on the gasket at the load condition *I* can be calculated and compared to the limit provided by the standard, i.e.

$$\sigma_{GI} = \frac{\sum F_{tor}Y_{G0}P_{QRI} - \frac{\pi}{4}d_{Ge}^2F_{QI}Y_{QI} - F_{RI}Y_{RI}}{Y_{GI}A_{Ge}} \leq Q_{s,min,I}^{(L)} \tag{7}$$

If Eq. (7) is satisfied, then the leakage limit state does not occur. As a result, by working out Eqs. (5-7), we can derive the external force $F_{RI,}$

$$F_{RI} \geq \frac{\sum F_{tor}Y_{G0}P_{QRI} - \frac{\pi}{4}d_{Ge}^2F_{QI}Y_{QI} - Q_{s,min,I}^{(L)}Y_{GI}A_{Ge}}{Y_{RI}} \tag{8}$$

that corresponds to the leakage onset. Further details of this derivation and relevant symbols can be found in La Salandra et al. (2016).

This model seems to predict satisfactorily the experimental results of the testing campaign by Reza et al. (2014), where BFJs were loaded only axially. Nonetheless, BFJs present in the piping system under study are subjected to multiple actions, in agreement with the experimental testing presented in Subsection 4.1. As a result, the mechanical model takes into account the possible interaction between axial and shear loading. More precisely, the leakage force for a BFJ subjected only to the shear loading is supposed equal to the bolt shear strength T_u provided by EN 1993-1-8 (2005), i.e.,

$$T_u = n * \frac{0.6 * f_u * A_{res}}{\gamma_{M2}} \tag{9}$$

Additionally, based on the aforementioned test campaign, the relation between the combined axial and shear leakage loading is approximated as linear,

$$T = (N_u - N)\rho, \text{ where } \rho = {}^{T_u}/_{N_u}. \tag{10}$$

Eq. (10) is presented graphically in Fig. 16 and the reader can appreciate the favourable agreement between model and test data.

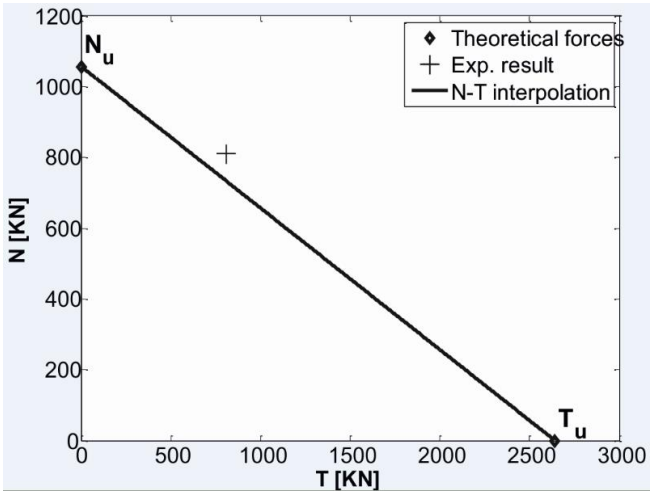

Fig. 16. Comparison between axial and shear leakage forces from the predictive model and experimental results.

Therefore, it is possible to calculate both axial and shear leakage forces of relevant BFJs under study, i.e. both 6'' and 18'' weld neck flanges, and relevant values are summarized in Table 4.

In order to accomplish the FE analysis presented in Subsection 6.3, we also needed to characterize BFJs in terms of axial and shear stiffness. With reference to the axial stiffness, we start from the mechanical model proposed in EN 1591 (2009). In particular, the mechanical model – sketched in Fig. 17 - considers the joint axial deformation δ_s due to an external force F_R as:

$$\delta_s = u_{an} + v_{an}. \tag{11}$$

where, u_{an} defines the bolt axial elongation and v_{an} identifies the axial deformation due to rigid flange rotation.

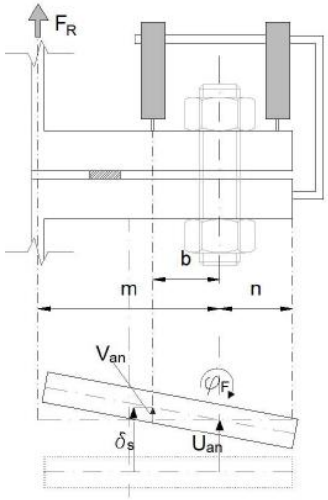

Fig. 17. Axial deformation model for BFJs.

Moreover, the equivalent shear stiffness K_s is estimated considering two plates of equal thickness *t* and joined by means of one bolt, i.e.

$$\frac{1}{K_s} = \frac{10t^3}{24E_b I_b} + \frac{4t}{3A_b G_b} + \frac{2tE_f}{t^2 E_f^2} \tag{12}$$

where the first and the second term on the right hand side refer to bending and shear compliance of the bolt, respectively; whilst the third term is related to the bearing compliance of plates. Finally, linear stiffness values for BFJs under study are collected in Table 4. As a result, BFJs add stiffness to the whole piping system under study.

Table 4
Axial and shear stiffness and leakage forces of BFJs.

	6'' Weld Neck Flange CL300	**18'' Weld Neck Flange CL150**
Axial stiffness [kN/mm]	14400	26000
Shear stiffness [kN/mm]	1270	4700
Axial leakage force [kN]	939	1034
Shear leakage force [kN]	2228	6097

With regard to leakage forces, one can notice that their values are significant; moreover, leakage due to shear needs greater force values.

4.3 Elbows performances

Piping elbows are critical component in a piping system and are characterized by a high flexibility, relevant level of stresses and strains and a significant cross-sectional deformation. Since the goal of this study was the investigation of the onset of leakage triggered by seismic action, particular attention was paid to pipe bends due to their vulnerability. Therefore, we focused on the identification of reliable EDPs related to leakage. Present regulations such as ASME BPVC (2004) do not explicitly treat leakage but consider "gross plastic deformation" instead. In particular, they are defined by means of the twice elastic slope (TES) method. In addition, very few papers are available on the topic; see Karamanos (2016) and Brinnel et al., (2016). A useful tool to classify the performance of piping elbows was developed by Vathi et al. (2015), which defines a set of damage levels, see in this respect Table 5, and the related limit states associated with several failure modes and relevant EDPs: they are collected in Table 6.

Table 5
Performance levels (after Vathi et al., 2015)

Level	**Description**
0	No damage
I	Minor (non-severe) damage
II	Major damage, but no loss of containment
III	Major damage with loss of containment

As stated before, our main interest was the LOC that corresponds to the Level III of damage.

Table 6
Failure modes with relevant EDPs and limit states (after Vathi et al., 2015)

Failure mode	EDP	Performance level and corresponding range	
Tensile fracture	Tensile strain ε_T	$\varepsilon_T < \varepsilon_\gamma$	0
		$\varepsilon_\gamma < \varepsilon_T <$ 0.5%	I
		0.5% $< \varepsilon_T < \varepsilon_{Tu}$	II
		$\varepsilon_T \geq \varepsilon_{Tu}$	III
Local buckling	Compressive strain ε_C	$\varepsilon_C < \varepsilon_\gamma$	0
		$\varepsilon_\gamma < \varepsilon_C < \varepsilon_{Cu}$	I
		$\varepsilon_{Cu} < \varepsilon_C < 5\varepsilon_{Cu}$	II
		$\varepsilon_C \geq 5\varepsilon_{Cu}$	III
Low-cycle fatigue cracking failure	Damage factor $D = \sum_i \frac{n_i}{N_i}$	$D < 0.5$	0
		$0.5 < D < 0.8$	I
		$0.8 < D < 1$	II
		$D > 1$	III

In particular, the threshold for tensile strain ε_{Tu} suggested by Vathi et al. is equal to 2%; conversely, to compute the same limit state for compressive strains, i.e. $5\varepsilon_{Cu}$, we adopted the following relationship,

$$\varepsilon_{Cu} = 0.5\left(\frac{t}{D}\right) - 0.0025 + 3000\left(\frac{\sigma_h}{E}\right)^2 \quad (13)$$

where *t* is the thickness of the pipe walls, *D* is the diameter, σ_h the internal pressure and *E* the Young's modulus. The leakage compressive strains for pipeline #1 and #6 are calculated by means of Table 2, where no internal pressure is considered to simulate the worst conditions. The resulting strain values are 3.6% for pipeline #1 and 4.7% for pipeline #6, significantly higher than the leakage tensile strain assumed to be 2%.

With regard to low-cycle fatigue defined in Table 6, we relied on the design low-cycle fatigue curves proposed by Otani et al., (2017), based on data derived from several experimental campaigns. Therefore, on the basis of the records 007162 and 006277, see Table 8, characterized by PGA of 1.04 g and 0.86 g, respectively, the seismic analysis on the plant was carried out. The corresponding time histories of elbow hoop strains were treated by means of a rainflow analysis. The subsequent application of the Palmgren-Miner rule entails damage values corresponding to D=8.52 10-5 and 8.89 10-5, respectively. On this basis and also in the case of some strong aftershock event, one can exclude LOC of elbows due to low-cycle fatigue failure.

In sum, the tensile strain can be considered the most important indicator of leakage in seismic assessment. This is also confirmed by the extensive test campaign conducted by the Japan Nuclear Energy Safety Organization and the Nuclear Power Engineering Corporation of Japan (JNES/NUPEC, 2008); and we recall the experimental work of Karamanos and co-workers that produced an overview of the mechanical behaviour of elbows, reporting analytical solutions, numerical results and experimental data. (Karamanos, 2016). As a result, we assume that piping elbows experience the onset of leakage when tensile hoop strains reach values of about 2% at the outer surface, in agreement with experiments. Indeed, studies by Singh and co-workers confirm that fatigue crack growth appears on the inside as well as the outside surface of the flank region (Singh et al., 2014).

5 FE modelling of LNG plant components and preliminary analyses

After the design of the BFJ mechanical model, FE modelling of other components in the LNG plant is reported in this section. For this purpose, the FE software ANSYS was employed.

5.1 LNG Storage Tank

The outer concrete layer of the storage tank was modelled by means of 4-node SHELL181 elements. In this respect, the design of the mesh was conceived with 34 elements along the circumference section, 19 elements along the wall height and 11 elements along the radius of the dome, as depicted in Fig. 18 (a). Moreover, the outer tank was fixed to the ground by means of rigid constraints. On the other hand, the inner steel tank was modelled by assigning the total mass of the LNG content when filled at the maximum capacity, i.e. 290,000 tons, to a single MASS21 element placed in the middle of the tank and connected to the concrete tank by means of 4 MPC184 Rigid Link elements; see Fig. 18 (b) in this respect.

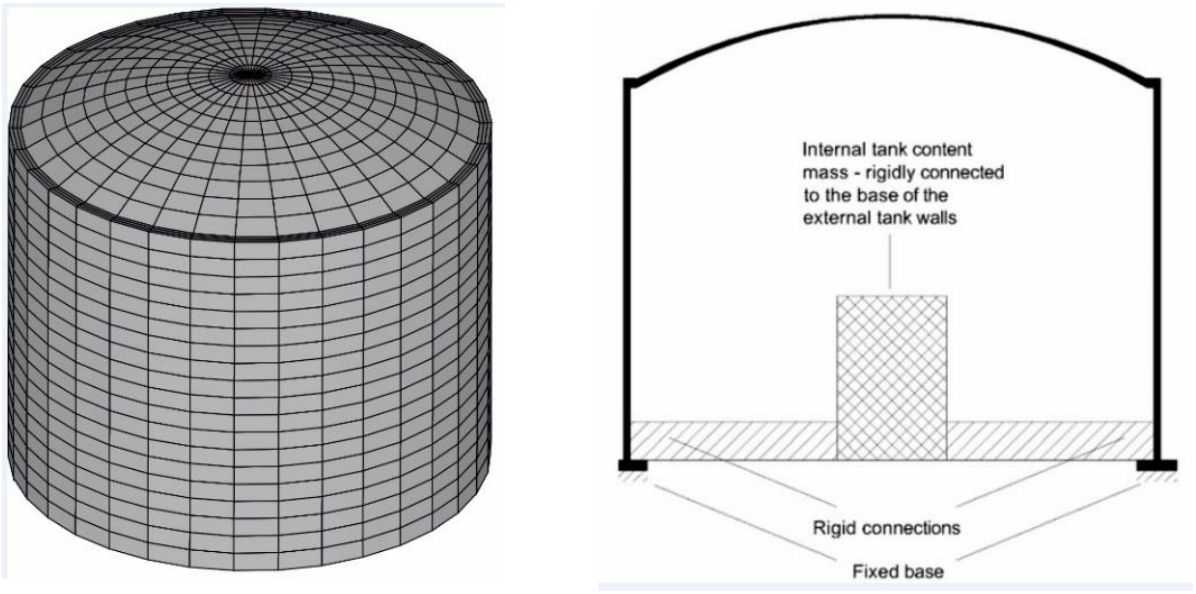

(a) (b)

Fig. 18. (a) Mesh design for the outer tank; (b) FE model of the inner tank.

The assumption of rigid walls is mainly due to the large outer tank thickness. Then, since forces generated by liquid modes (Malhotra et al., 2000) on the structure did not produce significant effects, we decided not to monitor local stresses on tank walls. Thus, from a dynamic point of view, we only take into account inertial effects of the LNG content in the calculation of reaction forces at the tank base.

5.2 Support Structures

The steel platform supporting piping systems and pumps, is on the top of the tank, as depicted in Fig. 19 (a). It is modelled by means of the BEAM4 and LINK180 elements for beams and axial members, respectively. All these elements are modelled with a linear constitutive law. On the other hand, the concrete support structure at the base of the tank is modelled with the same BEAM4 elements used for the steel platform. Moreover, it is rigidly constrained to the ground. In agreement with the Seismic Italian Standards (Norme Tecniche, 2008), the elastic modulus of concrete was reduced by 50 percent to account for cracking at the ultimate limit state. Nonetheless, during seismic analyses stress levels never

exceeded plastic limits in reinforced concrete elements. Therefore, a linear elastic constitutive law was considered also for this substructure.

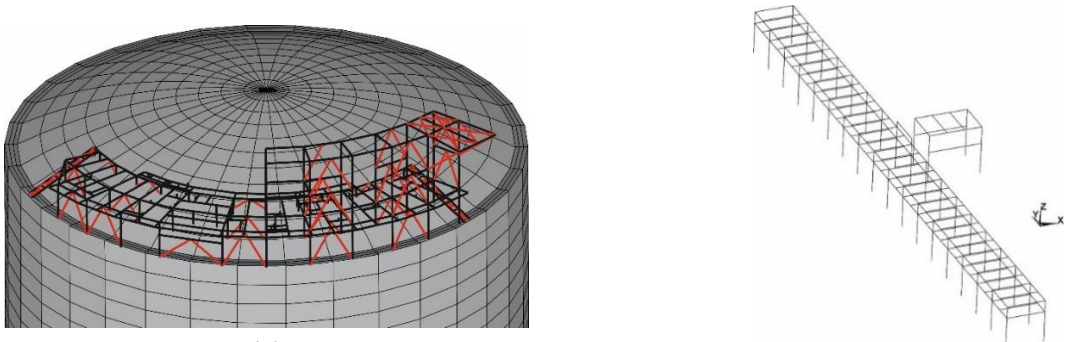

(a) (b)

Fig. 19. ANSYS FE model: (a) steel platform; (b) concrete support structure.

5.3 Piping System and Knock-Out Drum Area

The piping system was modelled by means of PIPE289 and ELBOW290 elements; these are both 3-node 3D elements with 6 DoFs per node. Lateral walls were modelled with SHELL181 elements with the shell thickness equal to the real pipe thickness. The design of the mesh was conceived with 20 shell elements along the circumference section. Furthermore, in order to correctly model the elbow constitutive law, the A312/TP304L stress-strain curve depicted in Fig. 20 (a) was reproduced with a bilinear relationship accounting for kinematic hardening.

Due to their complexity, only two of the seven pipelines on the steel platform on the tank dome were entirely modelled in ANSYS, i.e. pipeline #1 – the largest - and #6 – the smallest - as reported in Fig. 20 (b). Given the relevant involved weights, the unmodeled pipelines did not influence the dynamic response of the system. According to design requirements, two types of constraints were applied in modelling the contact between the piping system and the two support structures: i) a fixed constraint and ii) a roller allowing the piping to slide in its longitudinal direction.

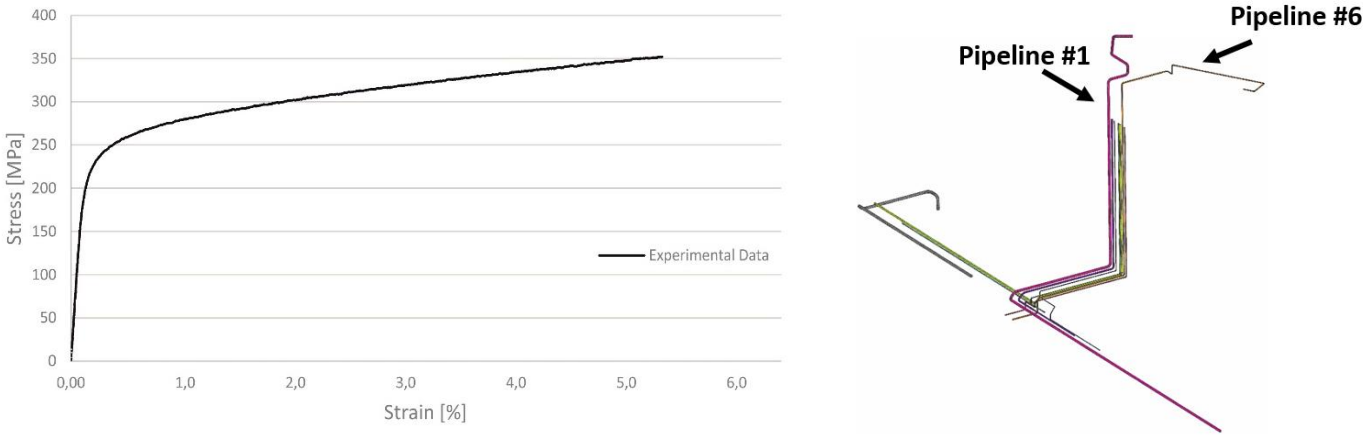

(a) (b)

Fig. 20. (a) Experimental results for A312/TP304L steel (b) FE model of the piping layout.

On the other hand, BFJs were modelled by means of a longitudinal and two transversal springs as presented in Subsection 4.2. To this end, and to take into account the different responses for tensile and compression forces, the

COMBIN39 element was used for the axial spring. The values of both longitudinal and shear stiffness for BFJs modelling are in Table 4.

Finally, the knock-out drum area is placed on the ground, close to the LNG storage tank, see Fig. 2 in this respect. The FE model developed by Kondorfer et al. (2016) was used for modelling both the pressure vessel C608 and the relative steel support structure. In particular, the support structure was modelled by means of BEAM4 elements, whilst the pressure vessel C608 was simplified with a mass-spring model, as depicted in Fig. 21.

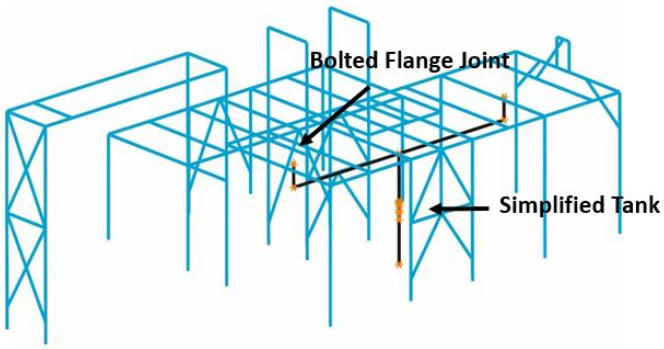

Fig. 21. FE model of Knock-out drum process area.

5.4 The whole ANSYS model

Once each single component was modelled, they were assembled to build up the complete FE model of the plant, as depicted in Fig. 22.

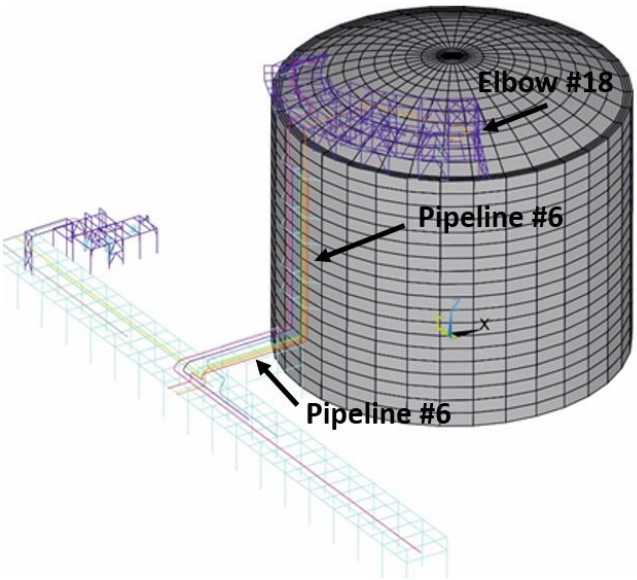

Fig. 22 ANSYS complete FE model of the LNG plant.

The complete model is highly complex, with totals of 19568 DoFs, 1338 BEAM4 elements, 159 PIPE289, 95 ELBOW290 and 1122 SHELL181.

5.5 Preliminary seismic analyses for boundary conditions and mesh sizes.

In order to assemble a FE model of the plant, a sensitivity analysis was conducted on important elements like tanks and elbows. As a result, the proper number of FE for the tank was set to 1122 shell elements; also, the number of

integration points along the wall thickness of elbows was selected equal to 2. The FE model was assembled considering the relative boundary conditions between the different components. In a greater detail we had to model the connections between: i) the knock-out drum area and the concrete support structure; ii) the steel platform and the dome of the LNG tank; iii) the two different sections of the concrete rack and the LNG tank; iv) the pipelines and the support structures. The first connection was made only by means of the pipelines that, coming from the support rack, were connected to the 18'' BFJs of the knock-out drum vessel; see, in this respect, both Fig. 7 and Table 4. The second connection was accomplished with rigid links coupling base nodes of the steel platform with nodes of the LNG tank dome. This was done to simulate a fixed constraint between the tank and the platform. The third coupling, like the first one above, was realised by the set of pipelines running through the different components. With regard to the last set of links, it is well known that pipeline supports are not frictionless (Peng, 1989). For this reason, we employed two different types of constraint: fixed supports with all displacement blocked in the *FIXED* case; roller supports with free axial displacements in the *FREE* case.

Once assembled the entire FE model of the plant, we needed to define important parameters, such as the amounts of fluids in pipelines and the types of constraint on support structures. For the first parameter, two cases were defined: i) the "LNG" case, in which the mass of the fluid was included in the pipelines, ii) the "EMPTY" case where the liquid mass was neglected.

Finally, some preliminary seismic analyses were carried out with different scenarios; the results are reported in Table 7.

Table 7
Comparison between preliminary simulations.

Earthquake	Record ID	PGA	Pipelines content	Constraints	Max Axial Strain Detected
South Iceland (aftershock)	006334	3.84	EMPTY	FREE	0.32% - Pipeline #6 Elbow 15
South Iceland (aftershock)	006334	3.84	LNG	FIXED	0.32% - Pipeline #6 Elbow 15
L'Aquila Mainshock	IT0792	5.35	EMPTY	FREE	0.45% - Pipeline #6 Elbow 11
L'Aquila Mainshock	IT0792	5.35	LNG	FREE	0.45% - Pipeline #6 Elbow 11
L'Aquila Mainshock	IT0792	5.35	LNG	FIXED	0.45% - Pipeline #6 Elbow 11
South Iceland	006277	5.08	EMPTY	FREE	3.25% - Pipeline #6 Elbow 18
South Iceland	006277	5.08	LNG	FIXED	3.25% - Pipeline #6 Elbow 18

It can be seen that there are no large differences between simulations with the same earthquake input and different pipeline conditions; hence, in order to obtain fragility curves for elbows, all required simulations were carried

out considering the same conditions, i.e. the "LNG" case for the pipeline content and the "FREE" condition for pipeline constraints.

6 Probabilistic Seismic Analysis

In order to evaluate the probability of exceeding a certain *EDP i.e. P(EDP)* from Eq. (4), the conditional probability of exceeding a prescribed *EDP* given the intensity measure, *IM, i.e.* $P(EDP > C_{LS}|IM = im)$ must be estimated. There are several alternative non-linear dynamic analysis procedures available in the literature for characterizing the relationship between *EDP* and *IM* based on recorded ground motion waveforms, such as: i) Incremental Dynamic Analysis (IDA, see Vamvatsikos & Cornell, (2004)); ii) Multiple-Stripe Analysis (MSA, see Jalayer & Cornell, (2009)); and iii) the Cloud Method (Cornell et al. 2002). Both IDA and MSA are suitable for evaluating the relationship between *EDP* and *IM* for a wide range of *IM* values; however, their application is time-consuming in our context of the LNG plant, about three days per run, as nonlinear dynamic analyses are repeated -usually for scaled ground motions- for increasing levels of *IM*. Moreover, the Cloud method does not require any amplitude scale factor. In fact, scaling can entail incoherencies in the probabilistic model, especially when all three -X, Y and Z- different components of each waveform are used for seismic demand analysis (Mackie and Stojadinović, 2005). Therefore, a *Cloud Analysis* will be applied in the sequel.

6.1 Cloud analyses and seismic input

As a first step, we consider only one scalar *IM* in the *Cloud Analysis, i.e.* the PGA. In particular, we decided to avoid, in the initial phase of the study, the adoption of any spectral quantity because of the heterogeneity in the modal frequencies of the LNG plant substructures. However, the Cloud Analysis was later performed by considering as additional IM the spectral acceleration Sa(T). Accordingly, the LNG plant described in Section 5 is subjected to a suite of 36 ground-motion waveforms shown in Table 8, and the associated structural response parameters, as anticipated in Subsection 2., are denoted as D = {D_i, i = 1:n}. In particular, the *Cloud Analysis* is based on two main hypotheses: i) D is characterized by a lognormal distribution; ii) the expected D is modelled as a linear relationship in the logarithmic space of D versus the candidate *IM*, i.e.

$$E[lnD|IM] = a + bln(IM) \tag{14}$$

In particular, *a* and *b* are regression coefficients estimated with the least square method. Then, *a* and *b* let us set the main parameters of the probabilistic seismic demand model (PSDM), i.e.

$$\sigma_{lnD|IM} = \beta_{D|IM} = \sqrt{\frac{\sum_{i=1}^{n}[ln(D_i) - ln(a(IM_i)^b)]^2}{n-2}} \tag{15}$$

$$m_D = \left(\frac{C_{LS}}{a}\right)^{1/b} \tag{16}$$

$$\beta_D = \frac{1}{b}\beta_{D|IM} \tag{17}$$

where:

β_D and m_D are the dispersion and the median of *D* values that exceed the limit state level, indicated as C_{LS}.

Thus, the conditional probability that the demand *D* exceeds the limit state capacity C_{LS}, which is known as fragility function, reads,

$$P[D \geq C_{LS}|IM = im] = \Phi\left[\frac{ln(im/m_D)}{\beta_D}\right] \quad (18)$$

In order to cover different values of magnitude M_w and PGA, we chose the suite of ground motions from different European databases (ESM and ITACA). All three components, two horizontal and one vertical, were applied during the seismic analysis. In particular, we applied the strongest of the components along the X axis, as depicted in Fig. 2, since we required a more demanding load in the preliminary analyses. The record names and relevant characteristics are collected in Table 8.

Table 8

Natural records used for Cloud analysis.

Record Name	Record ID	Date	M_w	PGA [m/s^2]
L'Aquila Mainshock	IT0792	06/04/2009	6.3	5.352
L'Aquila Mainshock	IT0789	06/04/2009	6.3	3.947
South Iceland (aftershock)	006334	21/06/2000	6.4	4.123
L'Aquila Mainshock	IT0790	06/04/2009	6.3	4.793
Northern Italy	IT0049	17/06/1976	4.5	0.811
Friuli	IT0077	11/09/1976	5.8	2.29
Southern Italy	IT0231	16/01/1981	5.2	1.069
Umbria-Marche 3rd shock	IT0491	14/10/1997	5.6	0.435
Garfagnana	IT0157	07/06/1980	4.6	0.595
App. Lucano	IT0607	09/09/1998	5.6	0.427
Ancona	IT0009	21/06/1972	4.0	4.025
South Iceland (aftershock)	006349	21/06/2000	6.4	8.218
Ancona	IT0002	14/06/1972	4.8	5.309
Firuzabad	007162	20/06/1994	5.9	10.444
Gazli	000074	17/05/1976	6.7	7.065
Erzincan	000535	13/03/1992	6.6	5.028
South Iceland	006277	17/06/2000	6.5	5.083
Racha (aftershock)	000501	03/05/1991	5.6	4.989
Pyrgos	000558	26/03/1993	5.4	4.256
Kalamata (aftershock)	000419	15/09/1986	4.9	3.275
NE of Banja Luka	005651	13/08/1981	5.7	3.551
Ionian	006131	24/04/1988	4.8	2.705
Bovec (aftershock)	006247	06/05/1998	4.3	2.801
Kozani (aftershock)	006093	19/05/1995	5.2	2.601
Patras	001932	14/07/1993	5.6	3.337
Faial	007329	09/07/1998	6.1	4.12
Oelfus	005030	13/11/1998	5.1	1.439
Mt. Hengill Area	005149	24/08/1997	4.9	1.691
Mouzakaiika	000566	13/06/1993	5.3	1.428
Holt	005237	23/04/1991	4.7	1.212
Kremidia (aftershock)	002025	25/10/1984	5.0	1.766
Friuli (aftershock)	000707	11/09/1976	5.3	1.931
Valnerina	000246	19/09/1979	5.8	0.870
Izmit (aftershock)	006440	07/11/1999	4.9	3.449
Ancona	000030	14/06/1972	4.3	3.972
Strait of Gibraltar	000878	04/01/1994	4.9	0.596

The response spectrum of the strongest components of the natural records is depicted in Fig. 23.

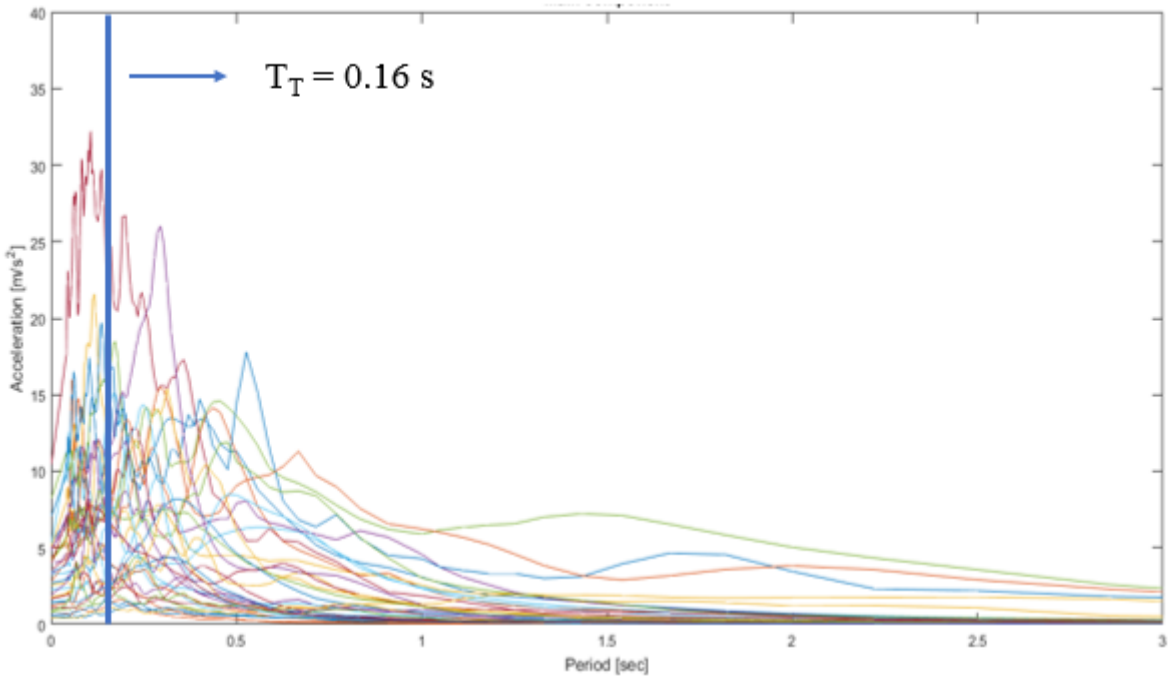

Fig. 23. Response spectra of the strongest components of natural records employed.

We can see the high variability of spectral acceleration; for instance, the values cover a wide range, from near zero to 3g. This wide range lets us evaluate and improve the efficiency of the PSDM accomplished in Subsection 6.4.

6.2 EDPs and Limit States

As anticipated in Subsection 1.1., because LNG is a hazardous material due to its flammability after vaporization, we must prevent component leakage under environmental hazards: i.e. earthquakes, in our particular case. Therefore, we focused our attention on leak-prone elements like BFJs and piping elbows. In this respect and in agreement with the PBEE framework described in Section 2, three EDPs, i.e. demands D in Eq. (4), were selected as listed in Table 9.

Table 9
EDPs description

EDPs Number	Parameter Description
1	BFJs Max Axial Force
2	BFJs Max Shear Force
3	Elbow Max. Tensile Hoop Strain

With regard to EDP1 and EDP2, leakage thresholds were discussed and defined in Subsection 4.2 and Table 3. Conversely, the onset of leakage in elbows was directly defined relating EDP3 to a value of tensile hoop strain according to the literature review and the analyses presented in Subsection 4.3. Relevant C_{LS} values – see Eq. (4)- associated with leakage thresholds are reported in Table 10 and EDP3 reads 2 percent for elbows. As a result to reach the LOC, piping elbows experienced several limit states corresponding to the different damage levels thresholds reported in Table 6. Nonetheless and in agreement with EN 1473 (2016), LOC is the most critical limit state for risk assessment and hazard tolerability classification of LNG plants, and therefore, we decided to perform a fragility analysis only for the LOC limit state.

Table 10
EDPs leakage limit states

	6” Flange [kN]	18” Flange [kN]
EDP1	939	1034

EDP2	2228	6097
	6” Elbows (%)	
EDP3	2	

6.3 Main results of FE analyses

With reference to BFJs and EDP1 and EDP2 values set in Table 10, the results of seismic analysis reveal that axial and shear forces do not approach leakage thresholds. Relevant values are shown in Fig. 24 for 6” and 18” flanges, respectively. A careful reader can notice that force values experienced by BFJs are substantially lower than limit leakage domains. Other limit states like yielding have not experienced both by flanges and bolts of FBJs.

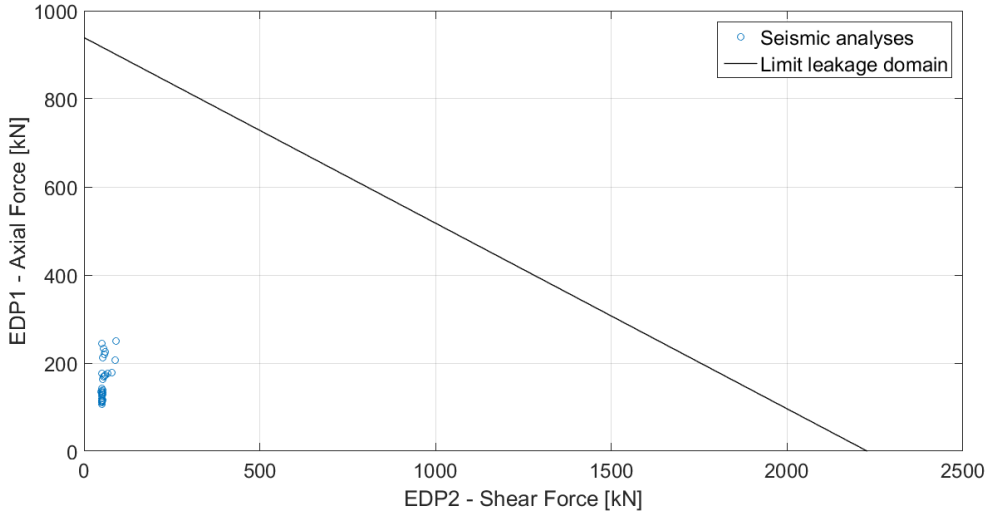

(a)

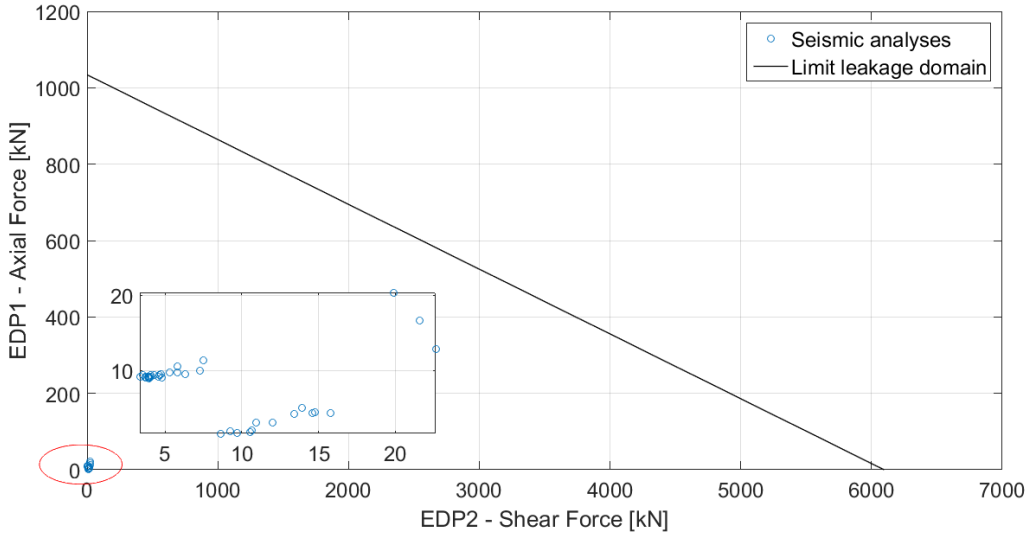

(b)

Fig. 24. Seismic analysis results for: a) 6” BFJs; b) 18” BFJs.

With regard to EDP3, both maximum and minimum absolute values of tensile hoop strains collected in Table 11 were detected for the Elbow #18 shown in both Fig. 11 and in Fig. 22.

Table 11

Maximum and minimum absolute values of EDP3

Record Name	Record ID	EDP3 - Elbow Tensile Hoop Strain [%]
Firuzabad	007162	4.77
Mt. Hengill Area	005149	0.106

These values are justified by the fact that Elbow #18 is located at about 40 m above ground on the steel platform that is built above the dome of the LNG tank; and relevant seismic forces are clearly significant. Therefore, we decided to introduce as additional IM, the spectral acceleration Sa(T) at the main vibration period of the LNG tank, i.e. T_T = 0.16 s, since we expect a stronger influence upon the EDP3 compared to the PGA. The values of Sa(T_T) can be observed in Fig. 23. Moreover, only one of three pipelines associated with pumps was modelled; other non-modelled elbows will likely be subject to similar seismic forces. However, we will consider these effects in the forthcoming subsection.

6.4 Efficiency analysis and fragility curves

According to Baker (2015), a PSDM is defined as efficient when the variance of the estimators is low; and in our particular case, the estimator is represented by lnD of Eq. (14). Given the results of the previous Subsection 6.3, only EDP3 was worthy of attention and, therefore, it was associated with the demand parameter *D*. Hence, we rearranged the seismic results as shown in both Fig. 25 and 26, and computed the coefficient of variation (COV) and the R^2 associated with (12). The PSDM based on the PGA achieved values of COV and R^2 equal to 0.6 and 0.6, respectively. These figures show that the correlation between PGA and EDP3 is relatively weak and associated with high dispersion (Mackie and Stojadinović, 2005, and Ebrahimian et al., 2015). On the other hand, the adoption of Sa(T) as IM, with COV and R^2 equal to 0.33 and 0.88, respectively, led to a very efficient PSDM involving a strong correlation on EDP3.

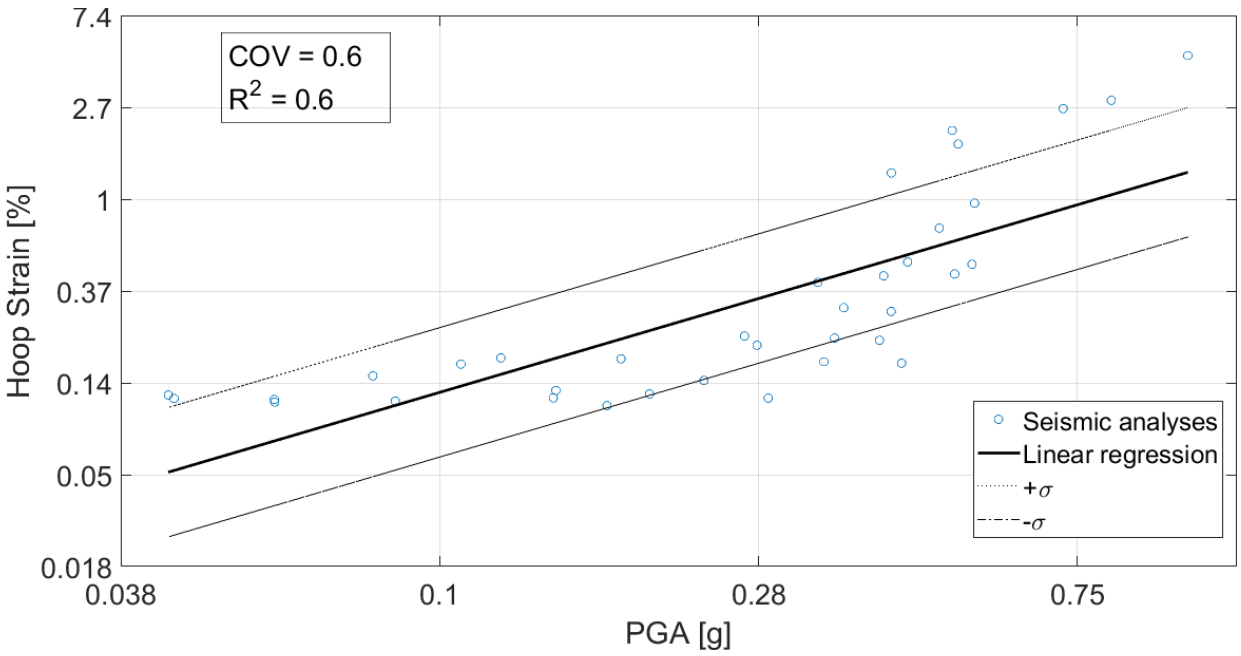

Fig. 25. Seismic analysis results and linear regression for EDP3 and PGA as IM.

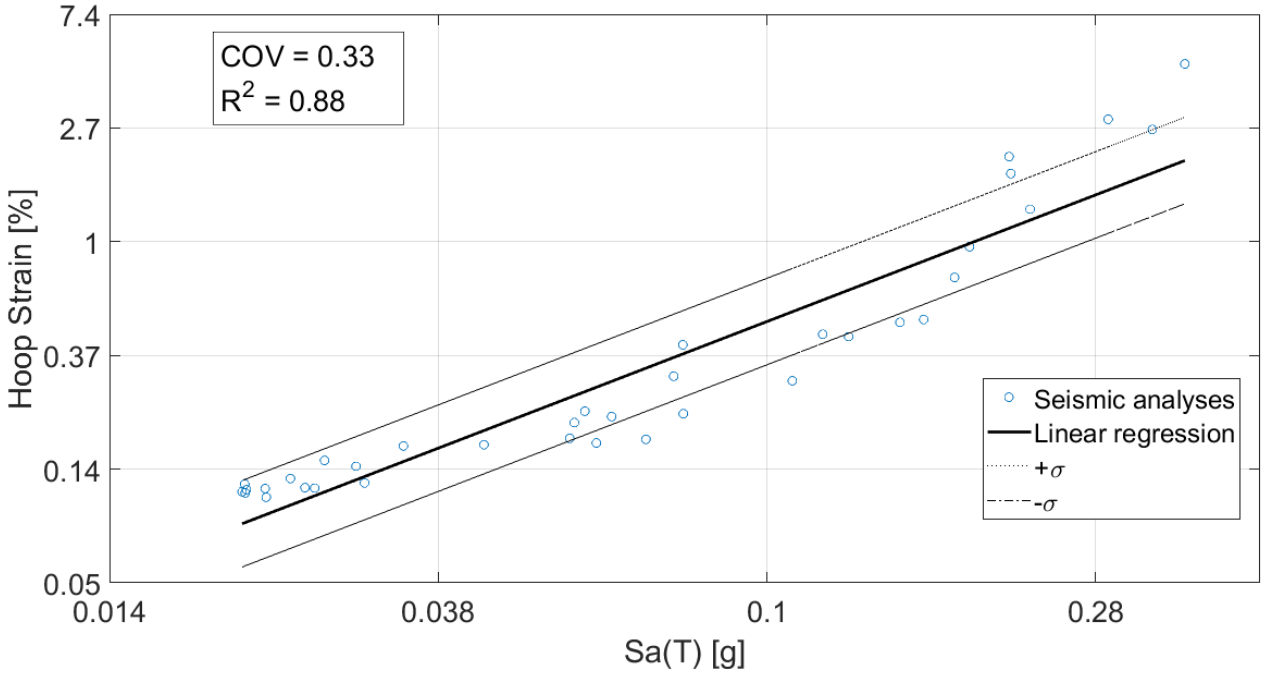

Fig. 26. Seismic analysis results and linear regression for EDP3 and Sa(T) as IM.

In order to proceed with a fragility analysis, we computed the fragility functions $F_D(IM)$, i.e. the probability of the demand D exceeding C_{LS} as,

$$F_D(IM) = P[D \geq C_{LS}|IM = im] = \Phi\left[\frac{ln(im/m_D)}{\beta_D}\right] \quad (19)$$

We note that $F_D(IM)$ was expressed using a lognormal cumulative distribution function (Baker, 2015). Both $F_D(PGA)$ and $F_D(Sa(T))$ of EDP 3 are reported in Fig. 27 and 28, respectively, whilst their parameters are listed in Table 12.

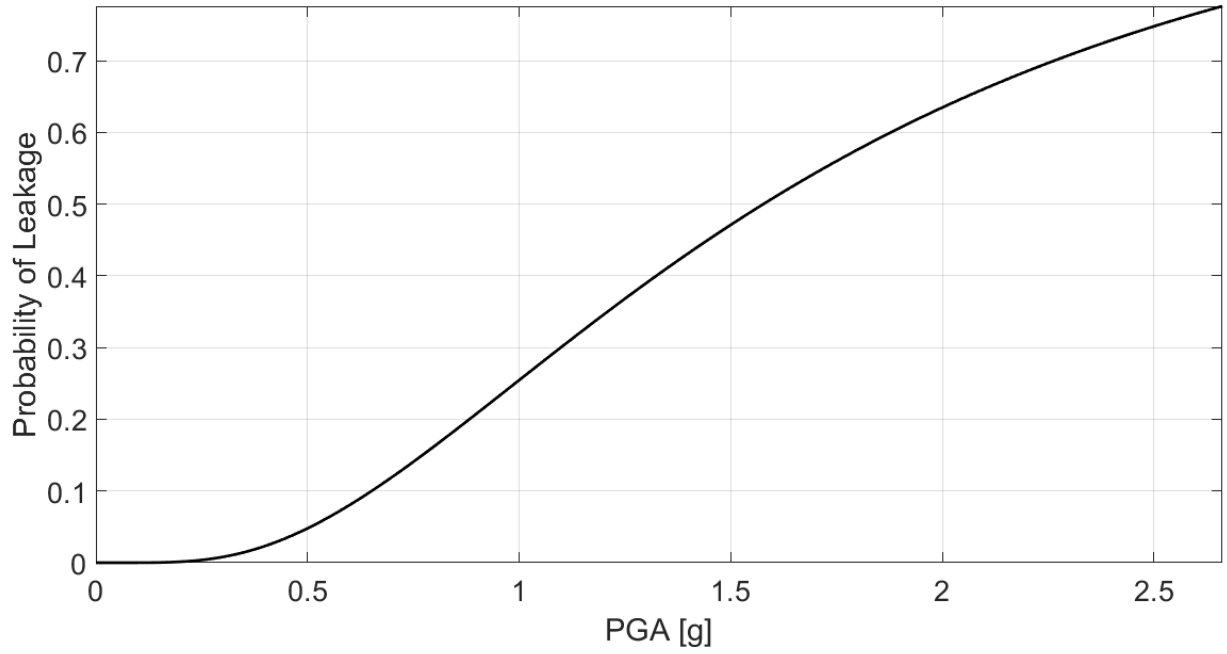

Fig. 27. Fragility curves for EDP 3 and PGA as IM.

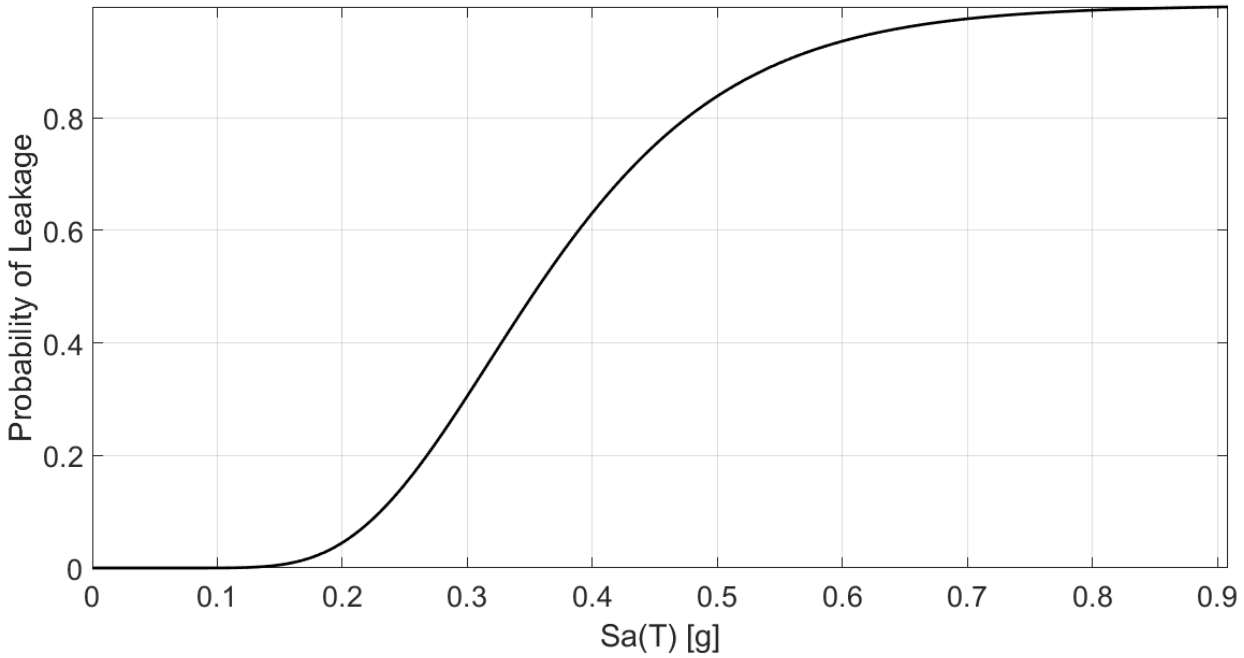

Fig. 28. Fragility curves for EDP 3 and Sa(T) as IM.

Table 12
Fragility function parameters

EDP	IM	Parameters	
		m_D	β_D
3	PGA	1.62	0.71
3	Sa(T)	0.345	0.342

As a result, both $F_D(PGA)$ and $F_D(Sa(T))$ exhibit a substantial vulnerability at low PGA levels even though $F_D(Sa(T))$ is significantly more severe. Moreover, the different values of the dispersion β_D expressed by (17), reflect the greater value of COV associated to PGA.

Given the fragility function $F_d(PGA)$ and the probability of failures involved in structural regulations EN 1990 (2002), i.e. $P_d = 7.2 \times 10^{-5}$ for ultimate limit states and $P_d = 6.7 \times 10^{-2}$ for serviceability limit states, it is important to estimate the relative annual probability *P(edp)* by means of Eq. (4): this read 1.38×10^{-5}. Nonetheless, we also calculated the leakage probability $P_n(edp)$ over the reference life of the LNG plant, i.e. 100 years by means of

$$P_n(edp) = 1 - (1 - P(edp))^n \tag{20}$$

where *n* defines the number of years. $P_n(edp)$ reads 1.4×10^{-3} and, compared to the aforementioned probability of failure values involved in EN 1990 (2002), we deduce that $P_n(edp)$ appears to be relatively high for LOC. It is worth noting that $P_n(edp)$ refers to the elbow of the pipeline connected to the pump column and located on the tank platform shown in Fig. 5. However, as stated in Subsection 3.5, the tank platform is characterized by 3 identical pump columns, each connected to one pipeline fitted with elbows. As a result, it is reasonable to assume that the leakage probability $\widetilde{P}_n(edp)$ referred to all three pipelines must be higher than $P_n(edp)$. In particular, if one assumes that LOC is considered as an independent event in each pipeline, then it follows that $\widetilde{P}_n(edp) = 3\, P_n(edp)$.

7 Conclusions

In this paper, we present a probabilistic seismic demand analysis of an LNG plant following the Performance-Based Earthquake Engineering procedure. In particular, first we evaluate the non-linear response of the whole LNG plant. Then we express the leakage risk of the most critical components of its pipeline network, i.e. elbows, by means of fragility functions. For this, we developed a mechanical model of bolted flange joints for leakage prediction, then calibrated by monotonic and cyclic joint testing.

With regard to the seismic response of LNG plant components, we found that bolted flange joints are relatively safe under seismic action, whilst elbows exhibit a significant degree of vulnerability.

Due to the complexity of LNG plant and the high computation demand by the FE model, we used the Cloud method for probabilistic seismic demand analysis. With regard to elbow response, we found that the maximum tensile hoop strain represents a suitable function for fragility analysis. Moreover, we show that fragility can be expressed as a function of peak ground acceleration of natural records. Nonetheless, the spectral acceleration evaluated at the period of the tank is more efficient due to the lower dispersion involved.

The results of fragility functions of elbows, i.e. the probability of leakage over the reference life of the plant of about 1.4×10^{-3}, demonstrates that the examined plant characterized by a reference life of 100 years would be at risk. Therefore, an adequate pipework design for LNG plants subjected to strong earthquakes is needed, especially for piping components on top of tall tanks.

Finally, given the limited number of leakage data of elbows and the two unmodeled pipelines connected to the LNG pump columns, both the effects of uncertainty in leakage thresholds and the correlation among damage levels of critical elbows on fragility functions deserve further investigation.

8 Acknowledgments

This work was carried out under a grant from the Research Fund for Coal and Steel of the European Commission within the INDUSE-2-SAFETY project: “Component fragility evaluation and seismic safety assessment of special risk petrochemical plants under design-basis and beyond-design basis accidents”, Grant No. RFSR-CT-2014-00025.

9 References

Abbiati G., Bursi O. S., Caracoglia L., di Filippo R., La Salandra V., 2016. Probabilistic Seismic Response of Coupled Tank-Piping Systems. Proceedings of the ASME 2016 Pressure Vessels & Piping Conference. PVP 2016, Vancouver, British Columbia, Canada, July 17-21, 2016.

ANSYS Mechanical Software by ANSYS, Inc. 2015, Southpointe 2600 ANSYS Drive Canonsburg, PA 15317 USA

Antonioni G., Spadoni G., Cozzani V., 2007. A methodology for the quantitative risk assessment of major accidents triggered by seismic events. Journal of Hazardous Materials 147, 48–59.

ASME. Boiler and Pressure Vessel Code Section VIII. New York, USA: American Society for Mechanical Engineers; 2004.

Baesi S., Abdolhamidzadeh B., Hassan R., Hamid M. D., 2013. Application of a multi-plant QRA: A case study investigating the risk impact of the construction of a new plant on an existing chemical plant’s risk levels J. Loss Prev. Process Ind., 26 (5), 924-935.

Baker JW, 2015. Efficient Analytical Fragility Function Fitting Using Dynamic Structural Analysis. Earthquake Spectra. Vol. 31, No. 1, pp. 579-599.

Barros da Cunha S., 2016. A review of quantitative risk assessment of onshore pipelines. Journal of Loss Prevention in the Process Industries 44, 282-298.

Brinnel V., Schaffrath S., Münstermann S., Feldmann M., 2016. Validation of a Concept for Burst Pressure Prediction by Damage Mechanics. Proceedings of the ASME 2016 Pressure Vessels & Piping Conference PVP. PVP2016, Vancouver, British Columbia, Canada, July 17-21, 2016.

Bursi O. S., Reza Md S., Abbiati G., Paolacci F., 2015a. Performance-based earthquake evaluation of a full-scale petrochemical piping system. Journal of Loss Prevention in the Process Industries, 33, pp. 10-22.

Bursi O. S. et al. 2015b, Report on seismic hazard for seismic input selection, Deliverable 1.2, INDUSE-2-SAFETY, Grant No. RFSR-CT-2014-00025.

Bursi et al., 2016a, Report on mechanical characterization of selected steel for cyclic loading and temperature sensitivity, Deliverable 4.1, INDUSE-2-SAFETY, Grant No. RFSR-CT-2014-00025.

Bursi, O. S., Reza S. et al., 2016b, "Component Fragility Evaluation, Seismic Safety Assessment and Design of Petrochemical Plants Under Design-Basis and Beyond-Design-Basis Accident Conditions", Mid-Term Report, INDUSE-2-SAFETY Project, Contr. No: RFS-PR-13056, Research Fund for Coal and Steel.

Campedel M., Cozzani V., Garcia-Agreda A., Salzano E., 2008. Analysis of major industrial accidents triggered by natural events reported in the principal available chemical accident databases. JRC Scientific and Technical Reports, EUR 23391 EN -2008.

Cozzani V, Antonioni G., Landucci G., Tugnoli A., Bonvicini S., Spadoni G., 2014. Quantitative assessment of domino and NaTech scenarios in complex industrial areas, Journal of Loss Prevention in the Process Industries 28, 10-22

Cornell CA, Krawinkler H. 2000. Progress and challenges in seismic performance assessment. PEER Center News, http://peer.berkeley.edu.

Cornell, C.A, Jalayer, F, Hamburger, R.O, and Foutch, D.A. 2002. Probabilistic Basis for 2000 SAC Federal Emergency Management Agency Steel Moment Frame Guidelines. ASCE Journal of Structural Engineering, 128:4, 526-533.

Nie J., DeGrassi G., Hofmayer C., 2008. Seismic Analysis of Large-scale Piping Systems for the JNES-NUPEC Ultimate Strength Piping Test Program. U.S. NRC NUREG/CR-6983, BNL-NUREG-81548-2008.

Ebrahimian H., Jalayer F., Lucchini A., Mollaioli F., Manfredi G., 2015. Preliminary ranking of alternative scalar and vector intensity measures of ground shaking. Bull Earthquake Eng 13, 2805–2840.

EN 1990 Eurocode – Basis of structural design. CEN 2002.

EN 1993-1-8. 2005. Eurocode 8: Design of steel structures – Part 1-8: Design of joints.

EN 1591-1. 2009. Flanges and their joints – Design rules for a gasketed circular flange connection – Part 1: Calculation method.

EN 1591-2. 2009. Flanges and their joints – Design rules for a gasketed circular flange connection – Part 2: Gasket parameters.

EN 1473. 2016. Installation and equipment for liquefied natural gas - Design of onshore installations.

Firoozabad E. S., Jeon, B. G., Choi, H. S., & Kim, N. S. 2015. Seismic fragility analysis of seismically isolated nuclear power plants piping system. Nuclear Engineering and Design, 284, 264-279.

GIE LNG Map, 2015, Gas Infrastructure Europe. www.gie.eu.

Hoseyni, S.M., Yousefpour, S., Araei, A.A., Karimi, K., Hoseyni, S.M., 2014. Effects of soil-structure interaction on fragility and seismic risk; a case study of power plant containment. Journal of Loss Prevention in the Process Industries, 32, 276-285.

IAEA, 2009. Evaluation of Seismic Safety for Existing Nuclear Installation. IAEA Safety Guide NS-G-2.13. International Atomic Energy Agency, Vienna.

I Y.T., Cheng Te-Lung, 2008. The development of a 3D risk analysis method. Journal of Hazardous Materials, 153, 600–608.

Jalayer F, Cornell CA, 2009. Alternative non-linear demand estimation methods for probability-based seismic assessments. Earthquake Engineering & Structural Dynamics, 38(8), 951-972.

JNES-NUPEC, 2008. Seismic Analysis of Large-Scale Piping Systems for the JNES-NUPEC Ultimate Strength Piping Test Program.

Karamanos S., 2016. Mechanical Behavior of Steel Pipe Bends: An Overview. J. Pressure Vessel Technology 138(4), Paper No: PVT-15-1165; doi: 10.1115/1.4031940.

Korndörfer J., Hoffmeister B., Feldmann M., 2016. Fragility Analysis of Horizontal Pressure Vessels in the Coupled and Uncoupled Case. Proceedings of the ASME 2016 Pressure Vessels & Piping Conference. PVP 2016, Vancouver, British Columbia, Canada, July 17-21, 2016.

Krausmann, E., Cruz, A. M., & Affeltranger, B., 2010. The impact of the 12 May 2008 Wenchuan Earthquake on Industrial Facilities. Journal of Loss Prevention in the Process Industries, *23, 2*, 242-248.

La Salandra V.; di Filippo R.; Bursi O. S.; Paolacci F.; Alessandri S., 2016. Cyclic Response of Enhanced Bolted Flange Joints for Piping Systems. Proceedings of the ASME 2016 Pressure Vessels & Piping Conference PVP. PVP2016, Vancouver, British Columbia, Canada, July 17-21, 2016.

Lanzano G., de Magistris S. F., Fabbrocino G., Salzano E., 2015. Seismic damage to pipelines in the framework of Na-Tech risk assessment. Journal of Loss Prevention in the Process Industries 33 (2015) 159-172.

Li X., Koseki H., Sam Mannan M., 2015. Case study: Assessment on large scale LPG BLEVEs in the 2011 Tohoku earthquakes. Journal of Loss Prevention in the Process Industries, 35, 257-266.

Li H. and Mackenzie D., 2006. Characterising plastic collapse of pipe bend structures. International Journal of Journal of Pressure Vessels and Piping 83 (2006) 85–95.

Mackie K. and Stojadinović B., 2005. Comparison of Incremental Dynamic, Cloud, and Stripe Methods for Computing Probabilistic Seismic Demand Models. Structures Congress 2005: pp. 1-11.

Malhotra P. K., Wenk. T., Wieland M., 2000. Simple Procedure for Seismic Analysis of Liquid-Storage Tanks. Structural Engineering International, 3/2000, pp. 197-201.

MATLAB and Statistics Toolbox Release 2015b, 2015, The MathWorks, Inc., Natick, Massachusetts, United States.

Norme Tecniche, 2008, “Norme Tecniche per le costruzioni,” DM Infrastrutture, 14 January 2008 (in Italian).

Otani et al.,2017, Seismic Qualification Of Piping System By Detailed Inelastic Response Analysis Part 2. A Guideline For Piping Seismic Inelastic Response Analysis. Proceedings of the ASME 2017 Pressure Vessels & Piping Conference PVP. PVP2017, Waikoloa, Hawaii, United States, July 16-20, 2017.

Park H.S., Lee T.H., 2015. Seismic Performance Evaluation of Boil-Off Gas Compressor in LNG Terminal. The Open Civil Engineering Journal, 2015, 9, 557-569.

Peng L.C., 1989. Treatment of Support Friction in Pipe Stress Analysis. Design and Analysis of Piping and Components, Vol. 169., Truong, O.N., Goodling, E.C., Bulashak, JR. J. J., Widera, G.E.O., Editors, PVP, ASME.

Reza M.S., Bursi O.S., Paolacci F., Kumar A., 2014. Enhanced seismic performance of non-standard bolted flange joints for petrochemical piping systems. Journal of Loss Prevention in the Process Industries, pp. 124-136 (vol. 30).

Singh P.K., Vaze K.K., Kushwaha H.S., Pukazhendi D.M., Seetharaman S., Murthy D.S.R., 2014. Experimental and Analytical Studies on Fatigue Crack Growth and Fracture Behaviour of Carbon Steel Elbows. 20th European Conference on Fracture, June-July 30-04, Trondheim-Norway.

Shome N., Cornell C. A., 1999. Probabilistic seismic demand analysis of nonlinear structures. Reliability of marine structures no. RMS-35, Stanford University, Department of Civil and Environmental Engineering

Vamvatsikos D, Cornell CA, 2004. Applied incremental dynamic analysis. Earthquake Spectra, 20(2), 523-553.

Vathi M., Karamanos S. A., Kapogiannis I. A, Spiliopoulos K. V., 2015. Performance Criteria for Liquid Storage Tanks and Piping Systems Subjected to Seismic Loading, Proceedings of the ASME 2015 Pressure Vessels & Piping Conference. PVP 2015, Boston, Massachusetts, USA, July 19-23, 2015.

Tondini N. and Stojadinoivc B., 2012. Probabilistic seismic demand model for curved reinforced concrete bridges. Bulletin of Earthquake Engineering, 10(5):1455-1479, 2012, doi 10.1007/s10518-012-9362-y.

Xie L. ,1998. The effect of multiple crack on the leak-before-break case of pipe. Int. J. Pressure Vessels and Piping. 75, 249-254.

Yang TY, Mohele J, Stojadinovic B, Der Kiuregan A. 2009, Seismic Performance Evaluation of Facilities: Methodology and Implementation. Journal of Structural Engineering, Vol. 135, pp. 1146- 1154.

Young, S., Balluz, L., Malilay, J., 2005, Natural and technologic hazardous material releases during and after natural disasters: a review. Sci. Total Environ. 322, 3-20.

Zerres, H., & Guerout, Y., 2004. Present calculation methods dedicated to bolted flange connections. International Journal of Pressure Vessels and Piping, 81, 211216.